FINITE ELEMENT MODEL FOR CRACK PROPAGATION IN A FRETTING FATIGUE PROBLEM

JUAN CARLOS MARTÍNEZ LONDOÑO

UNIVERSIDAD TECNOLÓGICA DE PEREIRA
FACULTAD DE INGENIERÍA MECÁNICA
MAESTRÍA EN INGENIERÍA MECÁNICA
PEREIRA
2016

FINITE ELEMENT MODEL FOR CRACK PROPAGATION IN A FRETTING FATIGUE PROBLEM

JUAN CARLOS MARTINEZ LONDOÑO

A thesis submitted in partial fulfillment of the requirements for the degree of Master of Science in Mechanical Engineering

DIRECTOR
LIBARDO VANEGAS USECHE
Ph.D.

UNIVERSIDAD TECNOLÓGICA DE PEREIRA
FACULTAD DE INGENIERÍA MECÁNICA
MAESTRÍA EN INGENIERÍA MECÁNICAPEREIRA
2016

Acceptance Page

_____
_____
_____
_____
_____
_____

_____
President, Graduate Committee

_____
Member, Graduate Committee

_____
Member, Graduate Committee

Pereira, Risaralda 13 de Mayo de 2016

Abstract

Fretting fatigue is a type of fatigue that may occur when two surfaces are in contact and subjected to a normal force together with a small, cyclic relative motion. As it may produce failure or reduce the lifetime of a component, it is important to study and model the fretting fatigue phenomenon. The Extended Finite Element Method (XFEM), which is a variant of the finite element method, is a suitable technique to model crack growth, because the mesh of the model may be independent of the crack path and, therefore, remeshing is not necessary for crack growth.

The objective of this thesis is to develop an XFEM model for crack growth under fretting fatigue conditions. The model is implemented in the software ABAQUS. The crack is represented as two-function levels using the level set method. A shifted enrichment formulation was implemented to define the contribution of the standard degrees of freedom plus the enriched contribution. The model includes a point-to-point formulation to set the contact between the crack faces. From the strain and stress results, the stress intensity factor is found using the interaction integral method, implemented in FORTRAN. Then, the crack propagation direction is determined by using the Maximum Tangential Stress (MTS) criterion and the minimum shear stress range criterion, and a new segment is added to the crack.

The model was validated with the results of similar works from the literature. The predicted crack using the MTS criterion was not similar to the validation information and it was not implemented in the final model. Finally, the model was implemented using data from a Chinese railway small scale fretting fatigue test for predicting crack growth, the predicted crack using the minimum shear stress range criterion proved to be an acceptable approximation for the real crack.

Acknowledgments

Deseo agradecer a mis padres, a mi hermana y a mi compañera sentimental por todo el apoyo, cariño y entendimiento que se me brindo durante el desarrollo de este trabajo.

Agradezco por la guía y ayuda al Doctor Libardo Vanegas Useche cuya dirección y aportes permitieron la culminación de este proyecto. Igualmente deseo agradecer al personal de la Universidad Tecnológica de Pereira donde se me prestó apoyo durante todo el desarrollo de este proyecto.

Agradezco al Doctor Eugenio Giner Maravilla docente de la Universidad Politécnica de Valencia por la explicación y la información prestada, ayuda que fue vital en el desarrollo de este proyecto.

Table of Contents

Abstract ii

Acknowledgments iii

Table of Contents iv

List of Figures vi

List of Tables viii

CHAPTER 1: INTRODUCTION 1

1.1 Justification 1

1.2 General Objective 2

1.3 Specific Objectives 2

CHAPTER 2: LITERATURE REVIEW 3

2.1 Introduction to Fracture Mechanics 3

2.1.1 History of Linear Elastic Fracture Mechanics 3

2.2 Fretting Fatigue 7

2.2.1 Contact Mechanics 9

2.2.2 Fretting Fatigue Stages 13

2.3 Introduction to Finite Element Modelling 21

2.3.1 The Strong and the Weak Form of a System 22

2.3.2 Hamilton's Principle 22

2.3.3 FEM Procedure 24

2.4 XFEM Basics 29

2.4.1 Crack Tip Enrichment 30

2.4.2 Heaviside Enrichment 31

2.4.3 Shifted Formulation 33
2.5 Methods to Determine the Stress Intensity Factor 33
2.5.1 Weight Functions 34
2.5.2 Local Methods 35
2.5.3 Energy Methods 36
2.6 Summary 40
CHAPTER 3: FEM AND XFEM MODELS 42
3.1 Introduction 42
3.2 XFEM Implementation in ABAQUS Program 42
3.2.1 User Defined Elements 43
3.2.2 Shifted Formulation and Overlay Elements 44
3.2.3 Element Crack Closure Method 45
3.3 XFEM Model 47
3.4 Files Description 50
3.4.1 Preprocessing 50
3.4.2 Processing 52
3.4.3 User Element Definition 54
3.4.4 Postprocessing 55
3.5 Summary 57
CHAPTER 4: RESULTS AND VALIDATION 58
4.1 Introduction 58
4.2 Validation of the Model 58
4.3 Results 66
CHAPTER 5: CONCLUSIONS AND FURTHER WORKS 76

5.1 Conclusions 76
5.2 Further works 77
CHAPTER 6. REFERENCES 79
APPENDICES 84

List of Figures

Figure 1. Fretting wear scars on AISI 304 after 105 cycles. (a) Partial slip (b) Gross slip. 9
Figure 2. Complete contact schematic. 10
Figure 3. Approximate stress distribution in a rigid flat indenter 11
Figure 4. Schematic representation of partial contact 12
Figure 5. Crack tip under mixed mode, MTS criterion. 18
Figure 6. Crack tip under mixed mode, Maximum Energy Release Rate criterion. 19
Figure 7. FEM design flow chart. 24
Figure 8. Example of a 2D mesh 25
Figure 9. FEM coordinate systems. 26
Figure 10. Crack tip enrichment. 30
Figure 11. Heaviside enrichment 31
Figure 12. Heaviside enrichment vectors. 32
Figure 13. Integral J contour definition 37
Figure 14. EDI Integral Domain 38
Figure 15. XFEM schematic 43
Figure 16. Standard XFEM crack closure 45
Figure 17. T2D2 node definition 46
Figure 18. Model geometry. 47
Figure 19. Model mesh representation 48

Figure 20. Model mesh zoom in crack zone 49
Figure 21. Applied loads in the numeric model 50
Figure 22. Initial crack stress distribution at the end of the first load step. 58
Figure 23. Initial crack stress distribution at the end of the second load step. 59
Figure 24. Near crack tip elements at the end of the second load step. 59
Figure 25. Initial crack stress distribution at the end of the fourth load step. 60
Figure 26. Near crack tip elements at the end of the fourth load step. 60
Figure 27. Initial crack stress distribution at the end of the sixth load step. 61
Figure 28. Near crack tip elements at the end of the sixth load step. 61
Figure 29. Fretting Fatigue Micrographs. 62
Figure 30. Predicted crack MTS criterion. 63
Figure 31. Crack path prediction P=40Mpa σ_{bulk}=110MPa 64
Figure 32. Crack path prediction P=80Mpa σ_{bulk}=130MPa 65
Figure 33. Crack path prediction P=80Mpa σ_{bulk}=150MPa 65
Figure 34. Crack path prediction P=160Mpa σ_{bulk}=190MPa 66
Figure 35. Rotatory bending test rig. 67
Figure 36. Test axle and wheel dimensions. 68
Figure 37. Scanning electron microscope image of fretting fatigue crack observed. 69
Figure 38. Axle and wheel model geometry 69
Figure 39. Axle and wheel model mesh zoom in crack zone 70
Figure 40. Applied loads in the axle and wheel model 71
Figure 41. Initial crack stress distribution at the end of the first load step, axle and wheel model 72
Figure 42. Initial crack stress distribution at the end of the second load step, axle and wheel model 73
Figure 43. Initial crack stress distribution at the end of the sixth load step, axle and wheel model 73
Figure 44. Crack path prediction, axle and wheel model 74
Figure 45. Crack path prediction- real crack micrograph superposition 75

List of Tables

Table 1. Mechanical properties Al7075-T6 49
Table 2. Pre-processing input files for ABAQUS X-FEM analysis.....51
Table 3. Loads and cycles to failure.....63
Table 4. Main mechanical properties of test axle and wheel materials 68

CHAPTER 1: INTRODUCTION

1.1 Justification

Industry is under the influence of the globalization and competitiveness. It is common to find longer work shifts, together with longer times between inspection and revisions. Crack initiation and propagation, as well as the probability of a catastrophic failure in a machine, are more susceptible to happen in this scenario.

The crack initiation and propagation phenomena are in most cases due to fatigue. This type of failure occurs in several industries, but it is of particular interest in the aeronautic industry, due to the fatal consequences that it has caused in the past. Although in some industries it is expected that a failure in a machine does not lead to a fatal consequence, it may increase the cost of operation, being this a suitable reason to develop studies about it.

The crack path prediction is an important step to create a more accurate fracture model. A more accurate solution can be used to take decisions in critical life extension problems. Also, it can be used to provide valuable information for the design of elements prone to fatigue failure.

The goal of this project is to develop a crack growth finite element model for fretting fatigue. The model will be developed with the help of the Soete Laboratory at Ghent University (Belgium), and the finite element software ABAQUS will be used. To achieve this goal, the project was divided into 2 steps. Firstly, crack initiation documentation and theories were studied to determine where the initial crack in a fretting situation is located. Secondly, crack growth theories were studied to determine the suitable ones to be implemented. The crack growth model will be developed for a certain piece geometry.

1.2 General Objective

To develop a finite element model for crack propagation under fretting fatigue.

1.3 Specific Objectives

- To review the literature and theory about strain and stress, fracture mechanics, and fretting fatigue.
- To study crack initiation and growth modeling, using the finite element method, under stresses due to fretting.
- To study crack modeling in the finite element software ABAQUS.
- To develop a finite element model for crack propagation under fretting fatigue.
- To validate and implement the model for a case study.

CHAPTER 2: LITERATURE REVIEW

2.1 Introduction to Fracture Mechanics

Fracture mechanics is one of the tools used to predict the possibility of failure of a component, its lifetime, and the safe loads for a certain lifetime, amongst others. It may be used for static loading, as well as for elements under cyclic load conditions. Fracture mechanics is a relatively new science, and, therefore, there is a great amount of research about it being conducted around the world.

Frequently, the fracture of structural components initiates at crack-type discontinuities in the material; these discontinuities can be induced in the manufacture of the components or be created in service. Historically, fracture mechanics has been used in cracked components to determine the load capacity and crack growth rate, with the objective of calculating the component lifetime after a crack is detected.

Fracture mechanics has led to the creation of methodologies for failure analysis. It considers certain mechanical properties: fracture toughness and plastic flow strength. These methodologies are especially helpful when they are used in low fracture toughness materials, in which the critical load for unstable crack growth is lower than the load for plastic collapse.

2.1.1 History of Linear Elastic Fracture Mechanics [1]

Fracture mechanics birth can be tracked to 1920 in a paper wrote by A. A. Griffith [2]; this article described the reason why the strength of fragile materials is smaller than the strength predicted by theory. The biggest advance proposed by Griffith was to relate the fracture stress σ_f with the crack size as shown in Equation 1.

$$\sigma_f = \sqrt{\frac{2\gamma E}{\pi a}} \quad (1)$$

where *E* is the Young modulus, 2γ is the surface energy term and a is half of the length of a central crack in a large plate (or the length of an edge crack), whose faces are normal to the tension applied. In the article, Griffith concluded that when cracks are present, stresses alone cannot be considered in a failure criterion. Taking into account that in an elastic continuum environment, the stresses will be infinite at the crack tips (i.e., crack fronts), Griffith did not focus on the high stressed zone at the crack tip, but he focused on an energy balance in the zone that surrounds it. Griffith´s work was supported by Obreimoff in 1930 [3], however, his work was unnoticed for some decades.

In the Soviet Union, between 1920 and 1940, there was an increasing interest in the problems related to fracture [4] [5]. G.V. Kolosov, N.I. Muskhelishvili, A. Yu. Ishlinsky, G.N. Savin, S.G. Lekhnitsky y L.A. Galin directed the mathematical school of elasticity and plasticity to contribute to the solution of important strength and fracture problems. In 1924, A.F. Joffe was the pioneer in the study of the fragile fracture related to the physics of crystal's cracks. In 1928, N.N. Davidenkov studied the influence of low temperatures in the elasticity of steel, to improve the understanding of fragile fracture in metals. In 1930, problems associated with wedge opened cleavage cracks in mica were investigated by P.A. Rehbinder y Ya.I. Fraenkel. At the same time, A.P. Alexandrov y S.N. Zhurkov were studying scale effects, as well as environmental effects, in connection with strength and fracture of glass fibers. In 1939 Westergaard proposed a stress function method for determining stresses near a crack.

In 1936, due to the threat of war in Europe, rebuilding the United States Naval fleet was in progress, and a new fast technique for fabricating ships was developed in a hurry. With this novel technique, 2700 all-welded hull ships were built during the war; approximately every seventh ship presented fractures, with 90 boats in

serious conditions, 20 totally fractured, and about 10 broken in two [6]. Fracture mechanics was the discipline called to explain the reason of these catastrophic incidents. Griffith's theories were available; however, it was considered applicable only to glass and brittle ceramics, because tests for engineering ductile materials showed that they fracture at higher stress levels than the ones predicted by Griffith theories.

Between 1937 and 1954, Irwin, heading the Naval Research Laboratory Ballistic Branch in Washington D.C, proposed that the Griffith theories could be modified to predict crack initiation in ductile materials. In 1945 Orowan's results from a study of the depth of plastic straining obtained using X-ray scattering for cleavage facets in low strength structural steel helped Irwin to introduce the loss of energy due to plastic deformation.

Irwin concluded that the energy loss on the surface was lower than the energy loss due to plastic deformation. Thus, the Griffith concept might be helpful and retained value for analysis, if the Griffith's surface energy was replaced by energy loss due to plastic strains occurring close to the crack tip. This idea was presented by Irwin in the ASM Symposium in 1947. Orowan presented the same idea in 1949, but regarded it as unlikely in structural materials; however, Orowan paper encouraged selection of a modified Griffith's concept as a promising starting point.

In 1957, Irwin suggested a stress-field parameter, the stress intensity factor K, to describe the stresses close to the crack tip, as shown in Equation 2, where r is the distance from the crack tip to the point analyzed

$$\sigma \, \alpha \, \frac{K}{\sqrt{r}} \tag{2}$$

Irwin established the relation between the energy release rate and *K*, assuming that the energy necessary to create new surfaces during crack growth comes from

the loss of strain energy of the elastic solid. Irwin defined the rate of energy loss as *G* in honor to Griffith; after that, he demonstrated that *G* could be calculated from the stress and displacement field in a region close to the crack tip [7].

Irwin stated that the parameter *G* measures the intensity of the stress field near the crack tip, provided that the plastic deformation is limited to a small region close to the tip. Irwin established the fracture toughness criterion (G_c), which indicates that the crack may grow if *G* reaches the value of G_c. He also described the influence of the thickness and the deformation ratio in G_c.

In 1957, Irwin used the half inversed Westergaard method to relate the *G* value with the stress field around the crack tip; he found the connection between the released energy and the stress intensity factor, as shown in equation 3, for plane stress, where *E* is the Young modulus:

$$K^2 = GE \tag{3}$$

To find *G*, Irwin suggested the use of deformation calipers, but his technique was not implemented until 30 years later when some uncertainty with the gradient and the region of domain of *K* was clarified. With this, a new method to found *G* was found using the deflection technique. The establishment of *G* and *K* as important parameters in cracked bodies makes it necessary to connect the stresses, strains, and displacements around the crack tip with these parameters.

Between 1945 and 1952 numerous writers present, under different load conditions, the stress distribution for tridimensional cracks in infinite bodies. Due to the relatively simple boundary conditions, exact solutions for these problems were found.

In 1957, Williams [8] developed a stress field analysis around the crack tip. This analysis focused on the global behavior of a simple crack, and it was independent

of the specimen. Williams introduced a series solution to the stress field around the crack tip; this series had singular superior order terms. These solutions apply to plain problems and have been used widely, even if the series integrity is still in debate.

This method has been proved to be helpful in boundary problems and finite element analysis. In 1958 Irwin wrote a paper with a review of the advances in fracture mechanics [9]. In this paper, expressions for strains and stresses at the crack tip under the three classic modes of loading can be found (opening, sliding, and tearing).

The progress reached up to 1960 was enough to guarantee the acceptation and continuous development of fracture mechanics. This was a consequence of the successful application of fracture mechanics basics into three emblematic problems. The emblematic problems were the high altitude explosions of the reaction planes “Havilland Comet” in 1953 and 1954, the fracture of a rotor of high capacity electric vapor generators in 1955-1956, and the failure of solid fuel rocket motors Polaris and Minuteman in 1957. All these failures were related to the introduction of new high performance high strength materials.

2.2 Fretting Fatigue

Fatigue is an issue to be taken into account in the moment of designing a mechanical structure or machine. The fatigue failure can be divided into two stages: a former stage of crack initiation and a later stage of crack propagation. The former stage consists of the formation of a very small crack, and it usually occurs in material discontinuities or high stress zones. To avoid these, designers tend not to use stress raisers like fillets, keyways, screw threads, and abrupt changes of section. These measures have been proved to be successful in flat homogenous surfaces; with these design conditions the presence of contact and

small slip amplitude between two bodies have shown to be a preferred crack initiation zone over a free surface. This phenomenon is known as fretting.

Fretting occurs whenever a coupling between two contact elements is under an oscillating force, and this oscillating force generates a relative tangential displacement over at least part of the interface. Fretting differs from sliding contact in that the tangential force does not result in global relative motion of contact surface, i.e., it results in partial slip. The contact zone can be divided into a micro-slip zone (25-100 μm) and a region with no relative motion (stick zone). [10]

The initiation process in fretting contact is a mixture of wear, corrosion, and fatigue phenomena. This initiation process can be divided into three stages [11]; the first stage involves the removal of the thin oxide layer covering the surface of the pieces through wear processes. As the oxide layer is removed new contact surfaces begin to adhere forming micro-welds or cold welds; the removed oxide generates an initial accumulation of wear debris between the surfaces. In support of this initial wear stage several researches [12] [13] have observed an increase in the coefficient of friction during the first few hundred cycles of fretting contact.

Additional operation cycles bring plastic deformation near the surface, wear, and formation of new oxides. The new created surfaces and metal debris are prone to oxidation. The near surface plastic deformation can generate the nucleation of micro-cracks in the material. At this point the combination of wear and fatigue phenomena accelerates the damage. The micro-cracks formation in the oxide layer can generate additional debris on the surface; this new debris has the potential of increasing the wear process, and at the same time the wear can accelerate micro-crack formation.

In the last stage, one or more of the nucleated micro-cracks propagate through the bulk material. As the crack propagates several microns away from the interface,

the contact stress becomes less influential, and the stress field generated by the bulk and global forces will dominate the process. [14]

2.2.1 Contact Mechanics

Mindlind [15], and afterwards Bryggman and Södeberg [16], distinguished three regimes of slip: elastic slip, plastic slip, and gross slip. Fretting fatigue will be predominant in partial slip and wear will be predominant in gross slip. The effect of partial and gross slip over the contact zone can be appreciated in Figure 1.

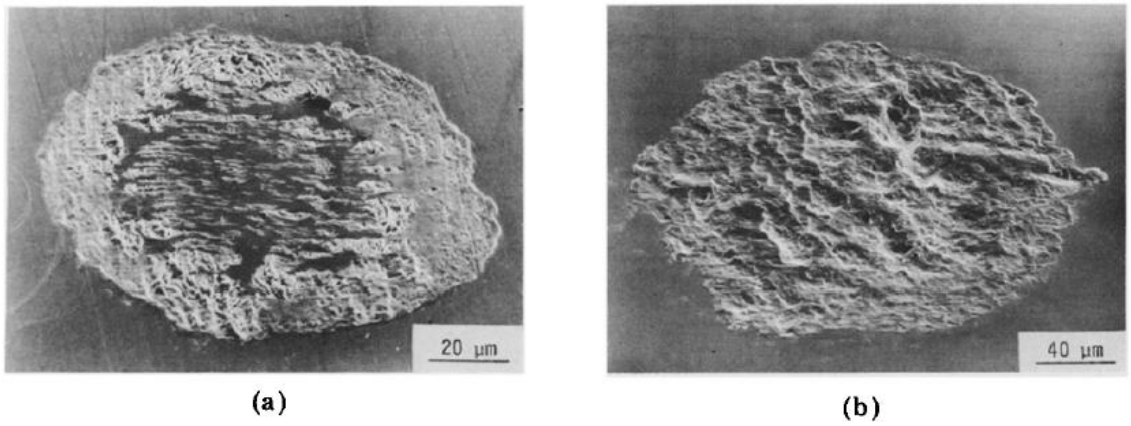

Figure 1. Fretting wear scars on AISI 304 after 105 cycles. (a) Partial slip (b) Gross slip.

Taken from: Bruggman and Soderberg [16]

In fretting fatigue tests, the contact between 2 cylinders (one of them may have infinite radius) is used when a proper stress approximation in the contact zone is needed, having also the possibility of finding it analytically. This contact is known as partial contact. However, its drawback is that not many real problems have this contact geometry.

2.2.1.1 Complete contact

Complete contact may occur in the interaction between two nearly plain surfaces. Many machines have this kind of contact, and fretting fatigue is the main failure mechanism. However, the complexity of the stress distribution makes it difficult to analyze this contact, and there are only approximate analytical solutions.

A typical complete contact model is shown in Figure 2, where *P* is the bulk load that keeps the indenter and the main piece in contact, *Q* is a tangential cyclic load on the indenter, and *σ* is a tangential cyclic stress in the main specimen.

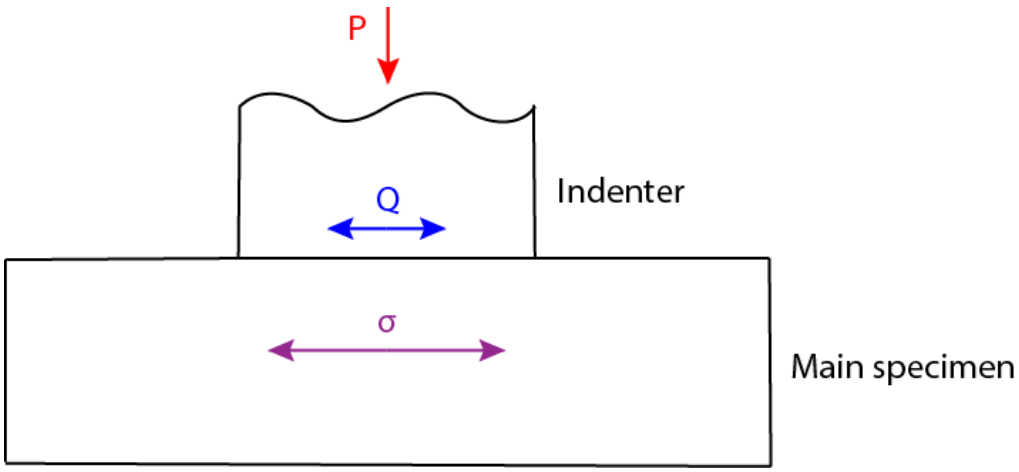

Figure 2. Complete contact schematic.

In their work, Hills and Nowell [10] found an expression to approximate the contact pressure for an indenter over a semi-infinite plane without friction, for the geometry shown in Figure 2.

$$p(x) = \frac{P}{\pi\sqrt{a^2 - x^2}} \tag{4}$$

In equation 4, *a* is half the length of the indenter and *x* is the distance from the center of the indenter. An approximate pressure distribution over the indenter can

be seen in Figure 3, where the dashed line is the approximation for the pressure distribution. It may be observed that the pressure tends to infinity towards the edges of the indenter. Diverse studies after Hills and Nowel [10] have been carried out considering complete contact conditions; several variables have been taken into account, such as rigid indenter, incompressible half-plane, indenter inclination, and geometry of corners. [17] [18] [19].

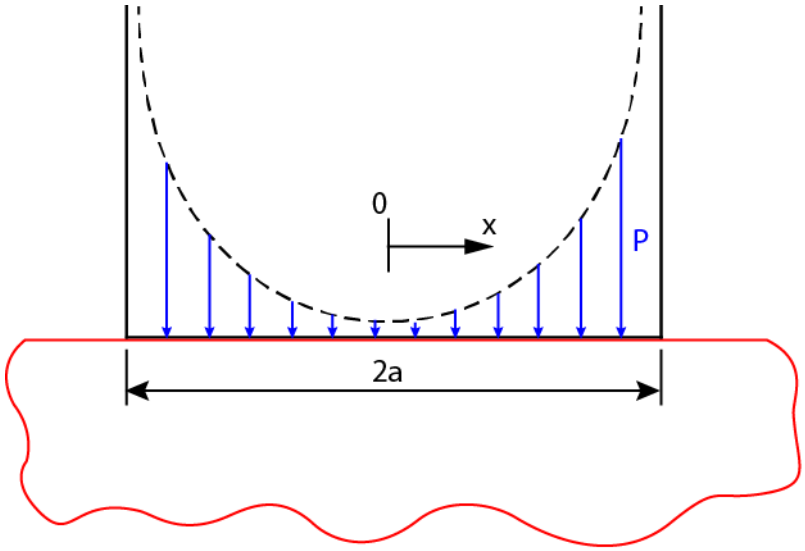

Figure 3. Approximate stress distribution in a rigid flat indenter

2.2.1.2 Partial contact

A typical partial contact model is shown in Figure 4. The contact is modeled as two cylinders in contact. A stick contact zone and a slip contact zone may be observed.

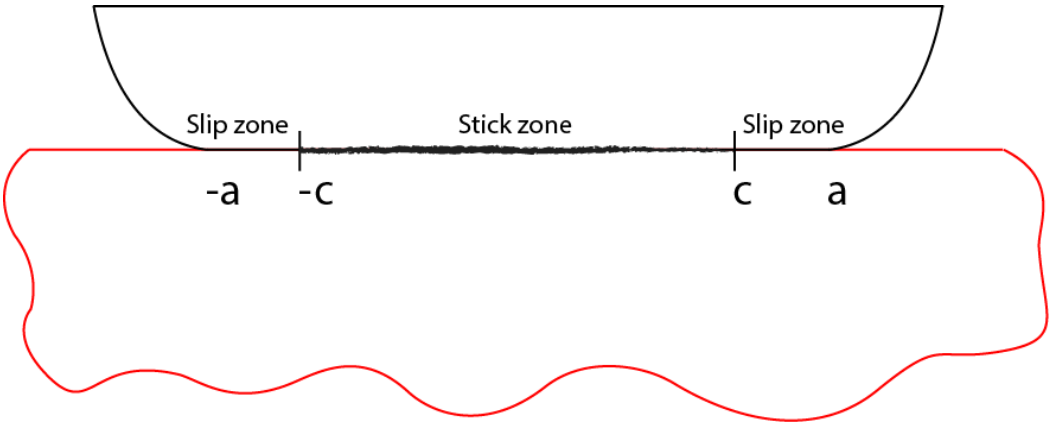

Figure 4. Schematic representation of partial contact.

Using the Hertzian contact for two cylinders and considering the conditions for contact proposed by Amontons and Coulomb [20], Equation 5 can be obtained:

$$\frac{c}{a} = \sqrt{1 - |Q/fP|} \tag{5}$$

where *P* is the bulk normal force between the bodies, *Q* is the frictional force and *f* is the Coulomb coefficient of friction. This equation can be used to found the approximate size of the stick and slip zones; this solution is known as the Mindlin solution, since the corresponding axisymmetric case was analyzed by Mindilin [15].

To analyze the stress distribution in this contact, a differentiation between three elliptical distributions must be done:

1. A distribution of normal pressure of peak magnitude $-p_o$ acting between $x = a$ and $x = -a$.
2. A distribution of shear traction of peak magnitude fp_o acting between $x = a$ and $x = -a$.
3. A second shear traction distribution of peak magnitude $-fp_o\, c/a$ acting between $x = c$ and $x = -c$.

For a linear-elastic analysis, the resultant stresses are the superposition of the three elliptical distributions. For example, to calculate the σ_{xx} component of stress at point (x, y) for a partial contact such as the one shown in Figure 4, transmitting normal and shear tractions, the superposition will have the structure shown in Equation 6.

$$\sigma_{xx}(x,y) = p_0 \left(\frac{\sigma_{xx}^{n}\left(\frac{x}{a},\frac{y}{a}\right)}{p_0} \right) + fp_0 \left(\frac{\sigma_{xx}^{t}\left(\frac{x}{a},\frac{y}{a}\right)}{fp_0} \right) + fp_0 \frac{c}{a} \left(\frac{\sigma_{xx}^{t}\left(\frac{x}{c},\frac{y}{c}\right)}{fp_0} \right) \quad (6)$$

where the functions in brackets can be obtained by analyzing the state of stresses and displacements with Hertzian contact formulation [21] [22]. A similar superposition can be performed to determine the displacements. Surface values are particularly important in fretting fatigue, since they allow to calculate the relative slip.

2.2.2 Fretting Fatigue Stages

As stated previously, a fretting fatigue process can be divided into two stages, an initial stage known as crack initiation or nucleation and a subsequent stage of crack propagation; in the next sections, these two stages will be analyzed.

2.2.2.1 Fretting fatigue crack initiation

Crack initiation is an important study area, since in many cases the life of a component is dominated by initiation. Initially, it is important to define what initiation is and distinguish it from the propagation phase.

The initiation step will vary depending on the observer and on the equipment available to detect the crack. However, regardless of the observer or the equipment, some considerations can still be taken into account. It is important to understand that the initiation is a continuous process and should not be taken as a

discrete process. Crack initiation is not an instant process; it takes time and the gradual accumulation of damage. While it is possible to say that there is no crack (or it is not detectable yet) before the loading and that a crack becomes detectable after a certain number of cycles, there is not a precise time at which it could be stated that the damage has become a crack.

Any description of the initiation process must be general and qualitative. Crack initiation occurs at a microscopic level, and it may be influenced by the local geometry, crystal orientation, and materials discontinuities, among others. The best conclusion that might be expected is to characterize the conditions in a general way and to predict where the initiation might occur.

In plain fatigue, cracks grow usually from a pre-existing flaw, such as a material void, inclusion, or geometry changes. If this is the case, there is no initiation period in the lifetime. If no flaw is present, it is necessary to accumulate a certain amount of damage to create a flaw where the crack can initiate. High stress zones are more likely to generate the damage, but in plain fatigue the stress changes softly with position; thus, it is hard to predict the exact zone where the crack will grow.

In fretting fatigue, the contact zone between the components generates an almost permanent high stress zone on its surfaces. The high stress zone is so localized that the crack initiation region can be predicted with a suitable degree of certainty. However, the stresses in the contact zone are so high that multiple crack initiation can be exhibited at the initiation region, in contrast to plain fatigue, in which almost always only one path occurs for the crack initiation process. Crack initiation in fretting fatigue takes place on the component surface; this is also usually the case for plain fatigue; however, a crack subsurface initiation may occur, starting at voids or inclusions [10].

Several studies have focused on uniaxial fatigue; these studies developed a suitable understanding of the many factors that influence fatigue. In the last years,

a new effort to understand the multiaxial fatigue has emerged; this, as a consequence of the complexity of the loads that a normal mechanical system is subjected. In consequence, multiple initiation criteria have been developed.

- **McDiarmid:** this fatigue failure criterion is based on a critical plane approach, where fatigue strength is a function of the shear stress amplitude and the maximum normal stress on the critical plane of maximum shear stress amplitude.

  The shear stress amplitude of the plane of maximum range of shear stress can be in the range $0.5t \leq \tau_a \leq t$, $0 \leq \sigma_{n,max} \leq \sigma_T$ as shown in Equation 7.

$$\tau_a/t + \sigma_{n,max}/2\sigma_T = 1 \tag{7}$$

  where τ_a is the shear stress amplitude of the plane, t is the reversed shear fatigue strength, $\sigma_{n,max}$ is the maximum normal stress on the plane of maximum range of shear stress and σ_T is the tensile strength [23].

- **Fatemi-Socie:** this fatigue failure criterion proposes a modification to Brown and Miller [24] critical plane approach to predict multiaxial fatigue life. The components of this modified parameter consist of the maximum shear strain amplitude and the maximum normal stress on the maximum shear strain amplitude plane.

  The proposed modification to Brown and Miller criterion is shown in Equation 8.

$$\gamma_{max}\left(1 + n\sigma_n^{max}/\sigma_y\right) = constant \tag{8}$$

where γ_{max} is the maximum shear strain, σ_n^{max} is the maximum normal stress on the maximum shear strain amplitude plane, σ_y is the yield strength and n is a constant obtained by fitting the uniaxial data against the pure torsion data [25].

- **Smith-Watson-Topper:** this criterion is based on the product of the first principal stress and the principal strain range for tensile mode failures; the parameter is defined in Equation 9.

$$SWT = \left(\sigma_1 \Delta\varepsilon_1 / 2\right)_{max} \tag{9}$$

where σ_1 is the first principal stress and $\Delta\varepsilon_1$ is the first principal strain range [26].

- **Crossland:** this is a stress based multiaxial fatigue criterion that uses the second invariant of deviatoric stress tensor and maximum hydrostatic stress as shown in Equation 10.

$$Cross = \sqrt{J_{2,a}} + \frac{I_{1,max}}{3}\left(\frac{3t}{b} - \sqrt{3}\right) \tag{10}$$

where $J_{2,a}$ is the amplitude of the second invariant of the deviarotic stress tensor, $I_{1,max}$ is the maximum of the first invariant of the stress tensor, t is the shear fatigue limit and b is the bending fatigue limit [27]**.**

2.2.2.2 Fretting fatigue crack propagation

The objective of a crack propagation analysis is to predict the direction and rate of crack growth under some known loads and geometry. In recent years, many studies for crack propagation with simple loadings have been carried out; as a

result, it is possible to predict the crack propagation direction and rate with some degree of confidence. For mixed-mode loading, as in fretting fatigue, the situation is different and the laws for crack direction and rate are still under study.

After the crack initiates, in early propagation stages the crack behavior is ruled by the frictional stress on the surface; the crack grows at an angle to the direction of the normal force and the crack propagation mode is plane sliding (mode II). After the crack grows beyond the neighborhood of the contact plane, the influence of the frictional stress is diminished, and the bulk stress will predominate over the crack behavior; the angle of the crack will be gradually reduced and eventually the crack direction will be normal to the contact zone. In this change of direction, a mixed mode between plane sliding and opening (mode I) will be present. At the final stage, the opening mode will prevail.

Next, some multiaxial crack propagation criteria will be reviewed.

- **Maximum Tangential Stress (MTS):** this crack propagation criterion considers, for brittle materials under gradually applied plane loads, that the crack extension starts at its tip in the radial direction (see polar coordinates in Figure 5) and the crack extension starts in a plane perpendicular to the direction of greatest tension; this means that the crack will grow from the tip in the direction in which the tangential stress $\sigma_{\theta\theta}$ is maximum and the shear stress is zero [28].

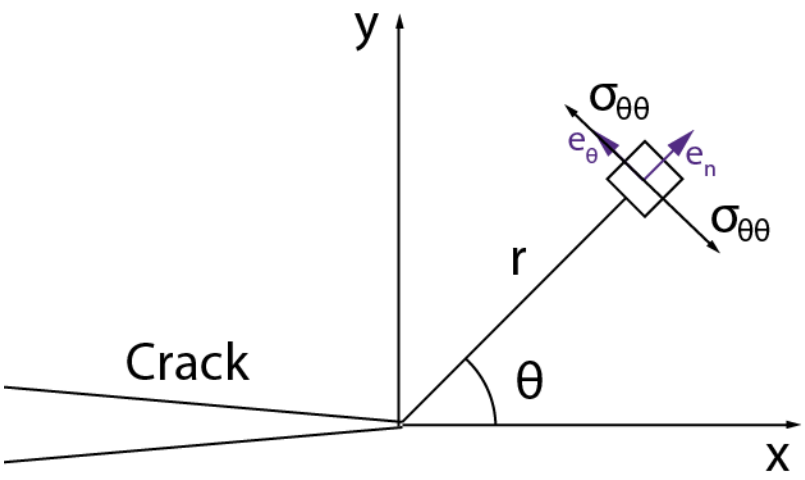

Figure 5. Crack tip under mixed mode, MTS criterion.

In a zone close to the crack tip (see Figure 5) the tangential stress can be expressed as a function of the stress intensity factors K_I and K_{II}:.

$$\sigma_{\theta\theta} = \frac{1}{\sqrt{2\pi r}} \cos\frac{\theta}{2}\left[K_I \cos^2\frac{\theta}{2} - \frac{3}{2}K_{II}\sin\theta\right] \tag{11}$$

The propagation angle can be determined as follows [28]:

E3

$$\theta_0 = \pm\arccos\left(\frac{3{K_{II}}^2 + \sqrt{{K_I}^4 + 8{K_I}^2{K_{II}}^2}}{{K_I}^2 + 9{K_{II}}^2}\right) \tag{12}$$

where the positive sign is used for negative values of K_{II}, and the negative one is used for positive values of K_{II}.

- **Maximum energy release rate:** this criterion suggests that the crack will propagate in the direction in which the energy release rate is maximum, and fracture will initiate when the release rate in that direction reaches a certain specified level. This criterion assumes that the crack propagates as a kink crack of length $a^* \ll a$, with origin in the crack tip, in a direction θ as shown in Figure 6.

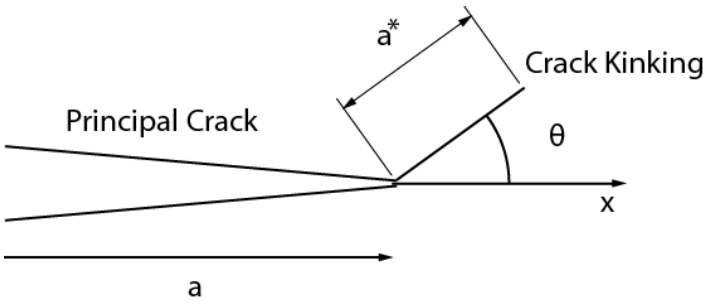

Figure 6. Crack tip under mixed mode, Maximum Energy Release Rate criterion.

In his work, Nuismer [29] proposed expressions to calculate the stress intensity factors in the kink crack K_I^* and K_{II}^* as a function of the stress intensity factors of the main crack K_I and K_{II} as follows:

$$K_I^* = C_{11}(\theta)K_I + C_{12}(\theta)K_{II} \tag{13}$$

$$K_{II}^* = C_{21}(\theta)K_I + C_{22}(\theta)K_{II} \tag{14}$$

where the C parameters can be obtained by.

$$C_{11} = \frac{1}{4}\left(3\cos\frac{\theta}{2} + \cos\frac{3\theta}{2}\right) \tag{15}$$

$$C_{12} = -\frac{3}{4}\left(\sin\frac{\theta}{2} + \sin\frac{3\theta}{2}\right) \tag{16}$$

$$C_{21} = \frac{1}{4}\left(\sin\frac{\theta}{2} + \sin\frac{3\theta}{2}\right) \tag{17}$$

$$C_{22} = \frac{1}{4}\left(\cos\frac{\theta}{2} + 3\cos\frac{3\theta}{2}\right) \tag{18}$$

Hussain *et al.* [30] proposed that the kink crack is formed at the angle θ, where the energy release rate $G^* = (K_I^{*2} + K_{II}^{*2})/E'$ attains a maximum, and the crack propagation initiates if G^* reaches the critical value G^c, where E' is E for plane stress and $E/(1-\nu^2)$ for plane strain, where ν is the Poisson´s ratio.

The loading in the small auxiliary crack is determined by the stress field near the crack with its intensity factors K_I and K_{II}; the factors K_I^* and K_{II}^* can be calculated, and the energy release rate obtained for a crack length a^* can be found by

$$G^*(\theta) = \frac{4}{E'}\left(\frac{\pi-\theta}{\pi+\theta}\right)^{\theta/\pi} \frac{1}{(3+\cos^2\theta)^2}[(1+3\cos^2\theta)K_I^2 + (4\sin 2\theta)K_I K_{II} + (9-5\cos^2\theta)K_{II}^2] \quad (19)$$

- **Strain energy density:** this is based on the angular dependence of the singular strain energy density U given by the stress field near the crack tip . In his work, Sih [31] proposed the following relationship

$$U = \frac{1}{2}\sigma_{ij}\varepsilon_{ij} = \frac{S(\theta)}{r} = \frac{1}{r}(a_{11}K_I^2 + 2a_{12}K_I K_{II} + a_{22}K_I^2) \quad (20)$$

where the strain energy density function $S(\theta)$ is expressed by three factors

$$a_{11} = [(1+\cos\theta)(\kappa-\cos\theta)]/16\pi\mu \quad (21)$$

$$a_{12} = \sin\theta\,[2\cos\theta - \kappa + 1]/16\pi\mu \quad (22)$$

$$a_{22} = [(\kappa+1)(1-\cos\theta) + (1+\cos\theta)(3\cos\theta-1)]/16\pi\mu \quad (23)$$

This criterion states that the crack extends in the direction θ_C in which the function $S(\theta)$ exhibits a minimum, and the crack propagates if $S(\theta_C)$ reaches a critical value S_C calibrated for mode I in plane strain. S_C can be obtained as:

$$S_C = \frac{1-2\nu}{4\pi\mu}K_{Ic}^2 \quad (24)$$

- **Minimum shear stress range:** this criterion is a generalization for non-proportional loading of the Cotterell and Rice [32] criterion of local symmetry. The latter criterion states that the crack will propagate in the direction where $K_{II} = 0$. For non-proportional loading, this cannot be attained, so the minimum shear stress range criterion proposes that the propagation will occur at the angle where the range ΔK_{II} is minimized [33].

  The computation of K_{II} must include the effect of friction traction on crack faces; where the domain and contour integral are proved to be inaccurate. In order to solve this, the angle of interest might be the one in which the shear stress range $\Delta\tau$ at the crack tip is minimum. The shear stress is developed in two orthogonal planes so that there are two orthogonal planes where $\Delta\tau$ will be minimum. The plane with the maximum $\Delta\sigma_n$ will define the crack growth direction because it will be the plane where less frictional energy is lost and there is more available energy for crack propagation.

2.3 Introduction to Finite Element Modelling

The beginning of finite element modeling can be found in the work of Richard Courant [34] in 1943. In his work, he used the Rayleigh-Ritz method and the method of finite differences to obtain approximately solutions to vibrating systems.

FEM for engineering applications was developed in the 1960s; this development was motivated by tasks of structural analysis in aviation, construction, and mechanical engineering. The formulation of the current FEM was achieved thanks to the works of Zienkienwicz, Turner, and Wilson (among others).

2.3.1 The Strong and the Weak Form of a System

The partial differential equations that model a system are known as the strong form of the governing system of equations for solids. The strong form requires a high continuity of the dependent field variables; the function of the field variable must be differentiable up to the order of the partial differential equations that are present in the strong form of the system equations. Usually, the exact solution of a strong form is very difficult for practical engineering problems, due to the complexity of the equations and the lack of continuity.

In contrast, the weak form of a system is an equivalent variational problem of a strong model; it is often of an integral form and requires a weaker continuity of the field variables. Due to the integral operation and a weaker requirement of the field, the weak form produces a set of discretized system equations that give more accurate results, especially for systems with complex geometry.

The weak form of a system is usually created using energy principles or weighted residual methods. The energy principles can be understood as a special form of the variational principle, which is particularly used for solid mechanics and structural problems. The weight residual method is a mathematical tool for solving all kinds of differential equations.

In the next section an energy principle, the Hamilton's principle, is introduced to subsequently use it to found the FEM formulation of problems of mechanics of solids and structures [35].

2.3.2 Hamilton's Principle

The Hamilton's principle states that: "Of all the admissible time histories of displacement the most accurate solution makes the Lagrangian functional a minimum". An admissible displacement must satisfy the following conditions:

- **The compatibility equations:** they ensures that the displacements are continuous in the problem domain.
- **The essential or the kinematic boundary conditions:** they ensures that the displacement constraints are satisfied.
- **The conditions at initial and final time:** requires the displacement to satisfy the constraint at the initial and final times.

In mathematical form, the Hamilton's principle can be written as

$$\delta \int_{t1}^{t2} L \, dt = 0 \tag{25}$$

Where t is time, δ is known as the variation of the integral path and the Langrangian L can be found as $L = T - \Pi + W_f$, where T is the kinetic energy, Π is the strain energy, W_f is the work done by external forces and.

The kinetic energy and the strain energy of the entire problem and the work done by external forces can be defined in the integral forms shown in the following equations.

$$T = \frac{1}{2} \int_V \rho \, \dot{U}^T \dot{U} \, dV \tag{26}$$

$$\Pi = \frac{1}{2} \int_V \varepsilon^T \sigma \, dV \tag{27}$$

$$W_f = \int_V U^T f_b \, dV + \int_{S_f} U^T f_s \, dS_f \tag{28}$$

where V is the volume of the solids; U, ε, and σ are the displacements, the strains obtained, and the field of stresses, respectively, of the admissible time histories; f_b

and f_s are the vector of forces and S_f represents the surface of the solid on which surface forces are prescribed.

2.3.3 FEM Procedure

As stated in a previous section, FEM is a powerful tool to design mechanical elements. A standard design process using FEM is an iterative process as shown in Figure 7.

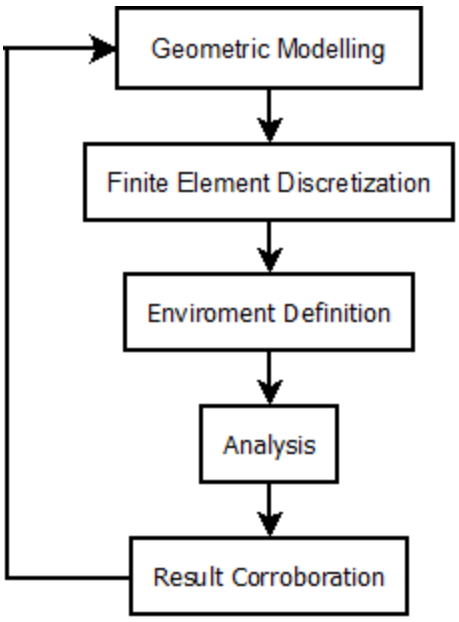

Figure 7. FEM design flow chart.

The geometric modelling consists of the creation of the mathematical model of the object or assembly. The geometry of the solid must be modeled with precision. In the finite element modeling, the geometry is divided into smaller discrete elements; also, in this stage, the properties of the materials and the elements are assigned. In the environment definition, the external loads and the boundary conditions are implemented in the model. At the analysis stage, the solution (strains, stresses, temperatures, etc.) of the model is obtained using the weak form of the problem. In the result corroboration, the solution achieved is tested with the design criteria to conclude whether a new iteration is needed.

The first three stages shown in Figure 7 are commonly named preprocessing, and the last stage post-processing. In the next sections, a more detailed description of the preprocessing and the analysis will be made [35].

2.3.3.1 Finite element discretization

In the finite element discretization, the element or the assembly is divided into a number of small elements. This procedure is often called meshing, which is usually developed using a so called preprocessor, especially for complex geometries. Figure 8 shows an example of a 2D discretization.

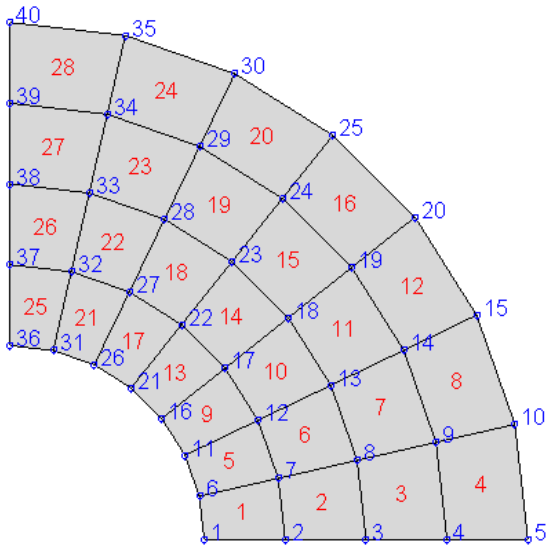

Figure 8. Example of a 2D mesh

Unique numbers are generated for all the subdivisions (elements) and nodes in a proper manner. An element is defined by connecting a number of nodes in a pre-defined constant shape; it is called the connectivity of the element. All the elements together must form the entire domain without gaps or overlapping (required condition for the Hamilton´s principle). It is possible to use different types of

elements with different numbers of nodes as long as they are compatible on the boundary between the elements.

The mesh density depends upon the accuracy required for the analysis and the computational power available. Commonly, a finer mesh will produce more accurate results, but the computational requirement will be increased; due this fact, normally the mesh will be non-uniform in the entire element; a finer mesh will be deployed in the zones where the displacements are bigger or more accurate results are needed.

2.3.3.2 Displacement interpolation

As in most physics problems, a FEM formulation is based on a coordinate system (*x*, *y*, and *z* in 3 dimensions). To formulate the FEM equation, a local coordinate system for an element is commonly defined, and a reference of it is made to a global coordinate system that is defined for the entire domain, as shown in Figure 9.

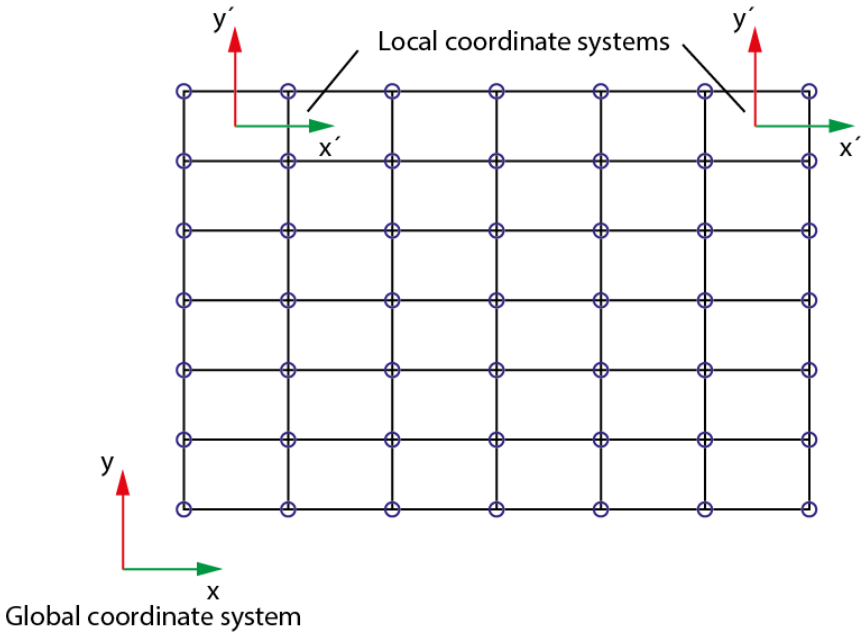

Figure 9. FEM coordinate systems.

Working in the local coordinate system, the displacements within the nodes U can be determined as an interpolation of the displacements of the nodes as shown in Equation 29.

$$U(x,y,z) = \sum_{i=1}^{n_d} N_i(x,y,z)d_i = N(x,y,z)d_e \tag{29}$$

Where n_d is the number of the nodes in the analyzed element, d_i is the nodal displacement vector at the ith node and d_e is the displacement vector for the entire element. Therefore, the total number of Degrees of Freedom (DOF) for the entire element is $n_d \times n_f$, where n_f is the number of DOF at a node.

N is a matrix of shape functions for the nodes in the element, which are predefined to assume the shapes of the displacement variations respect to the coordinates. It can be assumed that.

$$N(x,y,z) = \begin{bmatrix} N_1(x,y,z) & N_2(x,y,z) & \dots & N_{n_d}(x,y,z) \end{bmatrix} \tag{30}$$

where $N_i(x,y,z)$ is a submatrix of shape functions for displacement components.

2.3.3.3 Finite element equations in local coordinate system

Using the Hamilton's principle, the local coordinate system equations, and Hooke´s law, the finite element equation for an element can be written as.

$$k_e d_e + m_e \ddot{d}_e = f_e \tag{31}$$

where k_e is the stiffness matrix, m_e is the mass matrix and f_e is the element vector forces acting on the nodes. All these element matrices and vectors can be determined by integrating the given shape functions of displacement.

2.3.3.4 Assembly of global finite element equation

To assemble all the element equations, it is necessary to reference the local coordinate system equations to the global coordinate system; to do this, a coordinate transformation has to be performed for each element. The coordinate transformation gives the relationship between the element displacement vector in the local coordinate system d_e and the element displacement vector in the global coordinate system D_e as shown in Equation 32.

$$d_e = TD_e \tag{32}$$

where T is the transformation matrix, which can also be used to transform the force vector. The FE equation of all the elements referenced to the global coordinate system can be assembled in to form the global FE equation.

$$KD + M\ddot{D} = F \tag{33}$$

where K and M are the global stiffness and mass matrices, respectively, D is the displacement vector at all the nodes and *F* is the vector of the equivalent forces in the nodes. For constrained solid and structures, the constraints can be imposed by removing the rows and columns corresponding to the constrained nodal displacement.

A static analysis will involve the solution of the FEM without the term of acceleration $\ddot{D}$, so the FE equation for static analysis takes the form $KD = F$.

2.4 XFEM Basics

The standard finite element modelling is designed for continuous, singularity free problems; its application in fracture mechanics is limited due to the discontinuity introduced by the crack and the singularity in the crack tip. Some works tried to solve the problem with a special mesh distribution, where the discontinuity must align with the edge of the elements and a high mesh refinement must be performed in the zone near the discontinuity. It was proved that the problem can be solved for simple geometries and non complex load conditions [36]. In the standard finite element method, it is necessary to perform a remeshing every time the crack grows, causing high preprocessing times and computational requirements.

The Extended Finite Element Method (XFEM) is a numerical method that enables a local enrichment of approximation spaces. The method is useful for the approximation of solutions with pronounced non-smooth characteristics in small parts of the computational domain, for example, near discontinuities and singularities [37].

The crack discontinuities in XFEM can be modeled using two level set functions; a level set function is defined as a scalar function within the domain where the zero-level is interpreted as the discontinuity. As a consequence, the domain is subdivided into two by each level set function, where on either side of the discontinuity the level-set function is positive or negative [38]. The level set functions are independent of the mesh; therefore, only one mesh is necessary for all the crack growth steps. The interaction between the crack and the mesh is achieved by the enrichment of the nodes belonging to the elements intersected by the crack.

2.4.1 Crack Tip Enrichment

Belytschko and Black [39] proposed the enrichment of the nodes surrounding the crack tip; in Figure 10, the nodes with crack tip enrichment can be found as green squares.

.

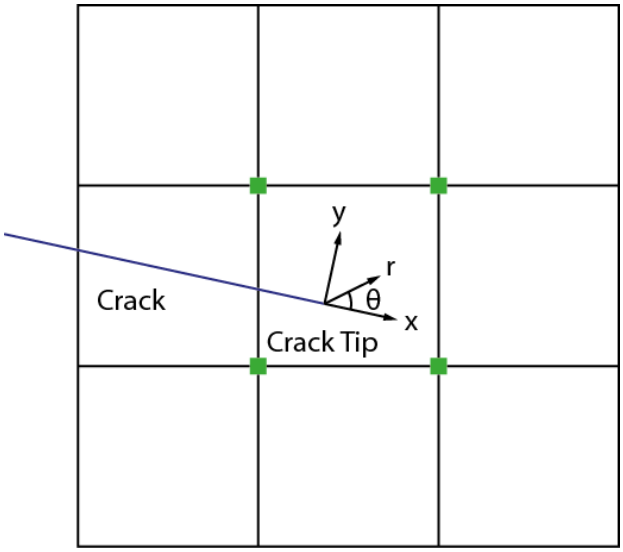

Figure 10. Crack tip enrichment.

The enrichment adds new DOF to the nodes, and the approximate finite element solution can be expressed as:

$$u_{FE}(x) = \sum_{i \in \Gamma} N_i(x) u_i + \sum_{i \in \Lambda} \left[N_i(x) \sum_{l=1}^{4} F_l(r,\theta) b_{il} \right] \tag{34}$$

Where Γ is the node set including all the mesh nodes, Λ is the node set of enriched nodes marked as green squares in Figure 10, $N_i(x)$ are the standard shape functions, b_{il} are the crack tip extra DOF and $F_l(x)$ are the crack tip functions defined as

$$F_l(r,\theta) = \left[\sqrt{r}\sin\frac{\theta}{2}, \sqrt{r}\cos\frac{\theta}{2}, \sqrt{r}\sin\frac{\theta}{2}\sin\theta, \sqrt{r}\cos\frac{\theta}{2}\cos\theta \right] \tag{35}$$

where r and θ are the local polar coordinates with origin in the crack tip and the x axis is aligned with the crack path. It can be seen that the singularity in the crack tip is introduced by the function $\sqrt{r}\sin\frac{\theta}{2}$, when θ is approaching to $\theta = \pm\pi$

2.4.2 Heaviside Enrichment

For longer or non-straight cracks, the crack tip enrichment of the nodes far away from the crack tip is not accurate, Moes *et al.* [40] proposed a complementary enrichment for non-crack tip nodes. The nodes belonging to an intersected element are enriched by the Heaviside function $H(x)$ as shown in Figure 11 (orange nodes).

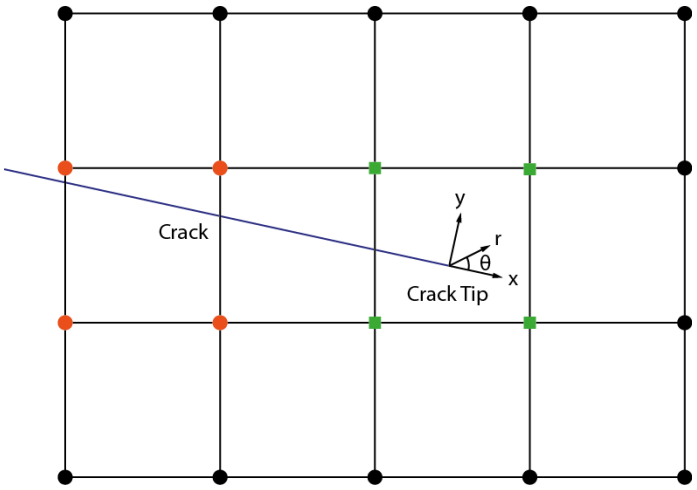

Figure 11. Heaviside enrichment

The Heaviside function is defined as

$$H(x) = \begin{cases} 1 & (x - x^*) \cdot e_n > 0 \\ -1 & (x - x^*) \cdot e_n < 0 \end{cases} \tag{36}$$

where x is the coordinate at the analyzed node, x^* is the coordinate of the nearest point in the crack, e_s (Figure 12) is the tangential vector in the crack growth

direction and e_n is the normal vector in the direction where $e_s \times e_n = e_z$, e_z pointing out of the paper.

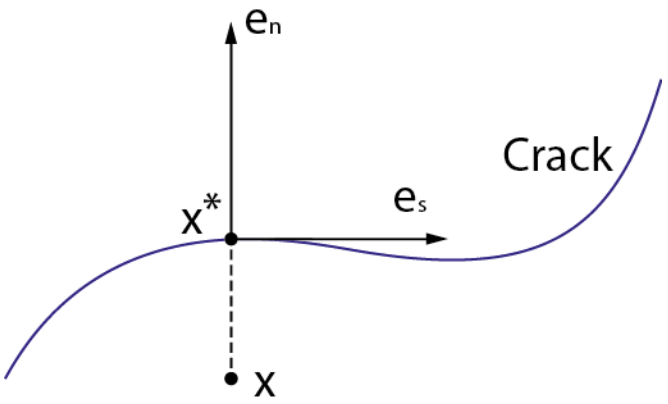

Figure 12. Heaviside enrichment vectors.

The finite solution including crack tip and Heaviside enrichments can be approximated as.

$$u_{FE}(x) = \sum_{i \in \Gamma} N_i(x) u_i + \sum_{i \in \Psi} N_i(x) H(x) a_i + \sum_{i \in \Lambda} \left[N_i(x) \sum_{l=1}^{4} F_l(r, \theta) b_{il} \right] \quad (37)$$

Where Γ is the node set including all the mesh nodes, Ψ is the node set with Heaviside enriched nodes (marked as orange circles), Λ is the node set of crack tip enriched nodes (marked as green squares), $N_i(x)$ are the standard shape functions, a_i are the Heaviside extra DOF, $H(x)$ is the Heaviside function, b_{il} are the crack tip extra DOF and $F_l(x)$ are the crack tip functions.

In summary, for an XFEM formulation in a two-dimensional problem, the standard nodes, marked as black circles in Figure 11, have 2 degrees of freedom (standard FEM degrees of freedom u_x, u_y), the Heaviside enrichment nodes have 4 degrees of freedom (standard FEM degrees of freedom u_x, u_y and Heaviside enrichment degrees of freedom a_1, a_2), and the crack tip nodes have 10 degrees of freedom (standard FEM degrees of freedom u_x, u_y and crack tip enrichment degrees of freedom b_1 to b_8).

2.4.3 Shifted Formulation

In the approximate solution described in the previous section, the displacement for an enriched node i is calculated as the contribution of the standard degree of freedoms plus the enriched contribution $N_i(x)H(x)a_i$ and/or $F_l(r,\theta)b_{il}$. It can be concluded that the standard degree of freedom u_i will not be a representation of the real displacement determined using X-FEM.

Zi and Belytschko [41] introduced the shifted formulation as a solution to make the standard degree of freedom u_i be the real displacement of the node. In this formulation, the extra degrees of freedom are nullified in the nodes (having the node coordinates x_i), the new approximate solution is.

$$u_{FE}(x) = \sum_{i\in\Gamma} N_i(x)u_i + \sum_{i\in\Psi} N_i(x)[H(x) - H(x_i)]a_i + \sum_{i\in\Lambda}\left[N_i(x)\sum_{l=1}^{4}[F_l(r,\theta) - F_l(r_i,\theta_i)]b_{il}\right] \tag{38}$$

2.5 Methods to Determine the Stress Intensity Factor

As mentioned in previous sections, the stress intensity factor is an important parameter for the study of crack initiation and propagation. Consequently, to calculate the stress intensity factor is one of the goals when a finite element analysis is implemented to solve fracture mechanics problems.

Numerous methods have been used to calculate the stress intensity factor; these methods can be divided into three large categories: weight functions, local methods, and energy methods.

2.5.1 Weight Functions

This method, originally proposed by Bueckner [42], has been proved to be a useful technique in determining the stress intensity factor. Afterwards, Rice [43] proved that the weight function is independent of the applied stress, based on the concept of elastic strain energy.

From Linear Elastic Fracture Mechanics (LEFM), it is known that the stress intensity factor K_I has a linear relationship with the applied load P. Using the principle of superposition in a system with multiple loads, the stress intensity factor can be calculated as:

$$K_I = \sum_{i=1}^{N} k_i P_i \tag{39}$$

Where k_i is the coefficient for the corresponding load P_i that contribute to the total stress intensity factor K_I and *N* is the number of loads

Bueckner [42] proposed, for a more general application, that the stress intensity factor K_I can be expressed as the product of the stress $\sigma(x)$ and the corresponding weight function:

$$K = \int_0^a m(x,a)\sigma(x)\,dx \tag{40}$$

Where a is the crack depth and $m(x,a)$ becomes the weight function at the position x and crack depth a. The determination of $m(x,a)$ requires a complex stress analysis of the cracked body and can be derived as:

$$m(x,a) = \frac{E'}{2K_r}\frac{\partial u^r(x,a)}{\partial a} \tag{41}$$

where $\partial u^r(x,a)$ is the displacement at the surface in the direction of $\sigma(x)$, r represents an arbitrarily given load system and $E' = E$ for plane stress and $E' = E/(1-\nu^2)$ for plane strain problems. E and ν are the Young´s modulus and Poisson´s ratio, respectively.

A number of researchers have been working on deriving an explicit expression or analytical form for the weight function $m(x,a)$ by approximating the displacement field. The most commons forms are shown in Equations 42 and 43.

$$m(x,a) = \frac{2}{\sqrt{2\pi(a-x)}}\left[1 + M_1\left(1-\frac{x}{a}\right) + M_2\left(1-\frac{x}{a}\right)^2 + M_3\left(1-\frac{x}{a}\right)^3 + \cdots + M_N\left(1-\frac{x}{a}\right)^N\right] \tag{42}$$

$$m(x,a) = \frac{2}{\sqrt{2\pi(a-x)}}\left[1 + M_1\left(1-\frac{x}{a}\right)^{1/2} + M_2\left(1-\frac{x}{a}\right) + M_3\left(1-\frac{x}{a}\right)^{3/2} + \cdots + M_N\left(1-\frac{x}{a}\right)^{N/2}\right] \tag{43}$$

2.5.2 Local Methods

Local methods are the procedures that allow finding directly the stress intensity factors; to achieve it, a precise representation of the displacement singularity in the crack tip is needed. Due to this fact, these methods are exclusively used in combination with singular elements, making these methods unlikely to be implemented together with XFEM.

The singular elements need a modification in the standard finite element formulation so that the stress intensity factor becomes a primary unknown, like the nodal displacement

The most common local methods are:

1. Displacement matching methods – extrapolation method [44]
2. Displacement correlation technique [45]
3. Quarter-point displacement technique [46]
4. Least-square method [47]

2.5.3 Energy Methods

Due to the complexity of calculating the correct strain field at the crack tip, Eshelby [48] defined a number of contour integrals that are patch independent by virtue of the theorem of energy conservation. Afterwards, Rice [49] noticed the importance of the J-Integral as a criterion for crack growth in fracture mechanics.

2.5.3.1 J Integral

Rice [49] originally defined the J integral for a homogenous elastic solid with no unloading, and no crack face traction. The integral is defined as.

$$J = \oint_{\Gamma} \left(W dy - t \frac{\partial u}{\partial x} d\Gamma \right) \tag{44}$$

Where Γ is a closed counter-clockwise contour starting from the lower flat notch surface and finishing on the upper flat surface, dΓ is the differential element of the arc length along the path, $t = \sigma_n$ is the traction vector on a plane defined by the outward normal n along Γ, and u is the displacement vector, as shown in Figure 13. W is the strain energy density:

$$W = \int_0^{\varepsilon} \sigma_{ij} d\varepsilon_{ij} \tag{45}$$

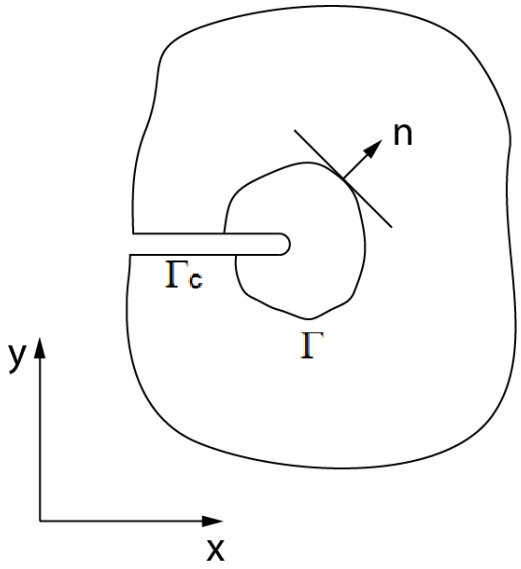

Figure 13. Integral J contour definition

It is noted that the equation is defined for a crack path in the *x*-axis direction. Rice [49] also proved that the J integral for an isotropic material is path independent. Also, it can be proved that the J integral is equivalent to the definition of the fracture energy release rate for linear elastic materials.

The original definition of J can be regarded as the first component of a more general path independent integral shown in Equation 46.

$$J_k = \int_{\Gamma} \left(W n_k - t \frac{\partial u}{\partial x_k} d\Gamma \right) \tag{46}$$

Or simply:

$$J_1 = \int_{\Gamma} \left(W dy - t \frac{\partial u}{\partial x} d\Gamma \right) \tag{47}$$

$$J_2 = \int_{\Gamma} \left(W dx - t \frac{\partial u}{\partial y} d\Gamma \right) \tag{48}$$

The generalized *J* also satisfies the Hellen and Blackburn relationship [50] for crack extensions parallel and perpendicular to the crack shown in Equation 49.

$$J = J_1 - iJ_2 = \frac{1}{E'}(K_I^2 + K_{II}^2 + 2iK_IK_{II}) \tag{49}$$

2.5.3.2 Equivalent Domain Integration (EDI) method

The implementation of the *J* integral as a contour integral is limited to relatively simple dimensional problems where the integral is path independent. However, the application for more general problems (three dimensional problems, dynamic, with thermal effects, etc.) supposes the definition of a path Γ infinitely close to the crack tip. The implementation of this path is not suitable for a FEM formulation due to the impossibility to follow the path due to restriction in the discretization and the induced error at the approximate solution near the crack tip.

Li *et al.* [51] proposed the equivalent domain integral method as a solution for this problem. The equivalent domain integration is defined at the domain A* showed in Figure 14.

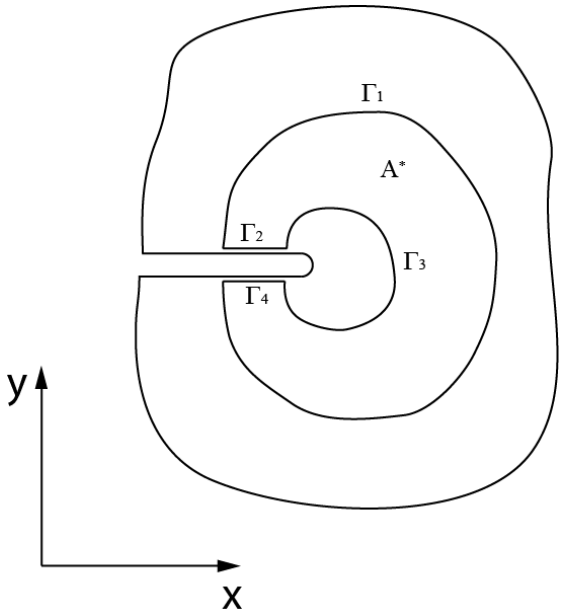

Figure 14. EDI Integral Domain

The integral can be defined as

$$J = \int_{A^*} \left[\sigma_{ij} \frac{\partial u_i}{\partial x_1} - W \delta_{1i} \right] \frac{\partial q}{\partial x_i} dA \tag{50}$$

where *q* is an arbitrary smoothing function that is equal to unity on Γ_3 and zero on Γ_1. The value of *q* within an element can be interpolated by.

$$q(x) = \sum_{i=1}^{n} N_i(x) q_i \tag{51}$$

where *n* is the number of nodes per element, q_i are the nodal values of *q*, and N_i are the shape element functions. The integral can be implemented for a FEM domain as.

$$J = \sum_{A^*} \sum_{g=1}^{ng} \left\{ \left[\sigma_{ij} \frac{\partial u_i}{\partial x_1} - W \delta_{1i} \right] \frac{\partial q}{\partial x_i} det \left(\frac{\partial x_j}{\partial \xi_k} \right) \right\}_g W_g \tag{52}$$

where *ng* is the number of integration points, *g* is each Gauss point, W_g is the Gauss weight factor and ξ is the crack path direction. In FEM the inner contour Γ_3 is often taken at the crack tip, so A^* corresponds to the area inside Γ_1. The boundary Γ_1 should also coincide with element boundaries.

2.5.3.3 Interaction integral method

The interaction integral method is a modification to the J integral used to find the stress intensity factor for mixed mode fracture; auxiliary fields are introduced and superimposed into the actual field satisfying the boundary value problem. These auxiliary fields are suitably selected in order to find a relationship between the

mixed mode stress intensity factors and the interaction integral [52]. The J integral for the sum of the two states can be defined as.

$$J = J^{act} + J^{aux} + M \tag{53}$$

where J^{act} and J^{aux} are associated to the actual and the auxiliary states and M is the interaction integral defined as:

$$J^{act} = \int_{A^*} \left[\sigma_{ij} \frac{\partial u_i}{\partial x_1} - W \delta_{1i} \right] \frac{\partial q}{\partial x_i} dA \tag{54}$$

$$J^{aux} = \int_{A^*} \left[\sigma_{ij}^{aux} \frac{\partial u_i^{aux}}{\partial x_1} - W^{aux} \delta_{1i} \right] \frac{\partial q}{\partial x_i} dA \tag{55}$$

$$M = \int_{A^*} \left[\sigma_{ij} \frac{\partial u_i^{aux}}{\partial x_1} + \sigma_{ij}^{aux} \frac{\partial u_i}{\partial x_1} - W^{M} \delta_{1j} \right] \frac{\partial q}{\partial x_j} dA \tag{56}$$

With the actual, auxiliary, and interaction works defined as.

$$W_s = \sigma_{ij} \varepsilon_{ij} \tag{57}$$

$$W^{aux} = \sigma_{ij}^{aux} \varepsilon_{ij}^{aux} \tag{58}$$

$$W^{M} = \frac{1}{2} \left(\sigma_{ij} \varepsilon_{ij}^{aux} + \sigma_{ij}^{aux} \varepsilon_{ij} \right) \tag{59}$$

The mode I and II stress intensity factors can be obtained choosing $K_I^{aux} = 1$, $K_{II}^{aux} = 0$, for mode I, and $K_i^{aux} = 0$, $K_{II}^{aux} = 1$, for mode II.

2.6 Summary

A literature review of fracture mechanics and fretting fatigue were carried out. Several theories for crack initiation and propagation were described. Crack initiation is not considered in the model to be developed. Two theories for crack

propagation were selected to be implemented the maximum tangential stress and the minimum shear stress range.

The theory of the finite element method and the modification known as extended finite method were studied. As the maximum tangential stress criterion needs the stress intensity factors to predict the crack path, some methods to determine the stress intensity factors were also shown. Due to its compatibility with finite element models the interaction integral method using domain integrals were chosen to be implemented to found the stress intensity factors.

CHAPTER 3: FEM AND XFEM MODELS

3.1 Introduction

In this chapter, a description of the developed XFEM model and its implementation in the software ABAQUS is carried out. Also, the model is implemented in a known geometry used by a field researcher.

3.2 XFEM Implementation in ABAQUS Program

In 2009, Giner *et al.* [53] implemented XFEM in ABAQUS; the article has a description of the model, and the user subroutines of the implementation can be found. This implementation allowed the modeling of multiple cracks with multiple orientations in two dimensions and fretting fatigue problems.

Figure 15 shows a schematic representation of the model developed in this work. In a first stage, known as preprocessing, the mesh is generated and the crack is represented as two-function levels using the level set method. Once the level functions are defined, the enriched nodes and elements are determined using the standard and user defined elements in ABAQUS. In a second stage, shown as analysis, the strains and stresses at the nodes are found. In the last stage, known as post-processing, the stress intensity factors are found using the interaction integral method implemented in FORTRAN. Once the stress intensity factors are found the crack propagation direction is defined and a new segment is added to the crack if needed.

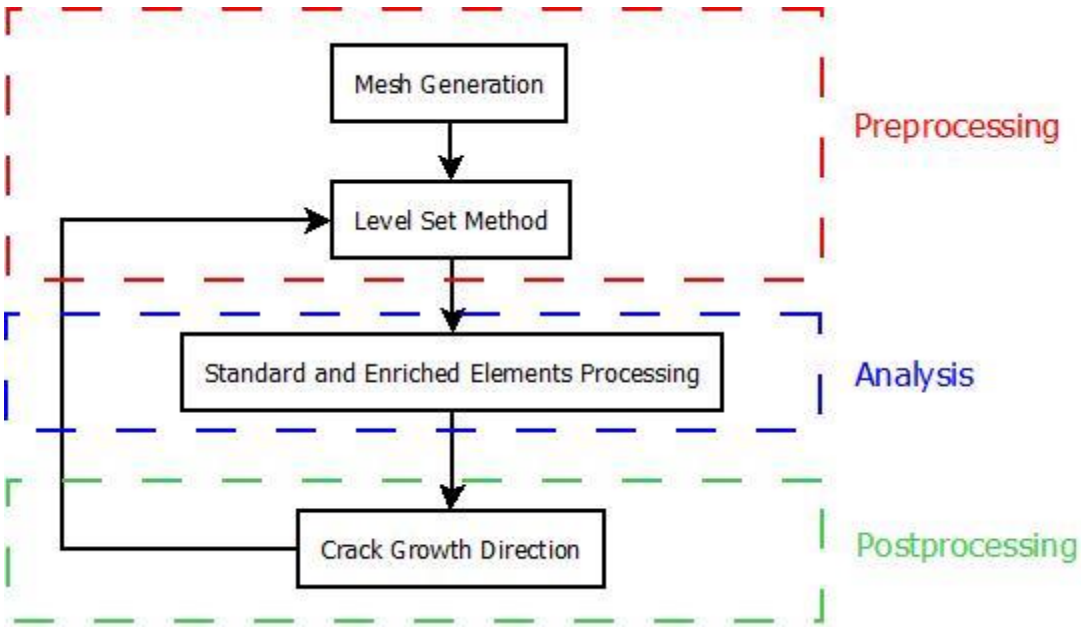

Figure 15. XFEM schematic

3.2.1 User Defined Elements

The user subroutines in ABAQUS allow the program to be customized for particular applications; for example, user subroutine UMAT in Abaqus/Standard and the user subroutine VUMAT in Abaqus/Explicit allow constitutive models to be added to the program, while user subroutine UEL in Abaqus/Standard allows the creation of user-defined elements.

The User Defined Elements (UEL) can be finite elements in the usual sense of representing a geometric part of the model, but they also can be used to solve linear and non-linear systems in terms of nonstandard degrees of freedom.

For a general user element in ABAQUS, user subroutine UEL may be coded to define the contribution of the element to the model. ABAQUS calls this routine each time any information about a user-defined element is needed. At each call, ABAQUS provides the values of the nodal coordinates and of all solution-dependent nodal variables (displacements, incremental displacements, velocities,

accelerations, etc.) at all degrees of freedom associated with the element, as well as the values, at the beginning of the current increment, of the solution-dependent state variables associated with the element. ABAQUS also provides the values of all user-defined properties associated with this element and a control flag array indicating which functions the user subroutine must perform. Depending on this set of control flags, the subroutine must define the contribution of the element to the residual vector, define the contribution of the element to the Jacobian (stiffness) matrix, update the solution-dependent state variables associated with the element, form the mass matrix, and so on. Often, several of these functions must be performed in a single call to the routine [54].

3.2.2 Shifted Formulation and Overlay Elements

ABAQUS software allows the modelling of the interaction between bodies (for example, bodies in contact) in engineering problems. In the modelling of contact, the degrees of freedom 1 and 2 represent the physical displacements of the node. Giner et al. [53] implemented the shifted formulation described in Section 2.4.3; in this formulation, the first two degrees of freedom (1 and 2) of the enriched nodes are the physical displacements as needed in the contact formulation.

Nowadays, ABAQUS does not post-process the information generated for user defined elements, so it is not possible for ABAQUS to plot these elements. To allow an approximate plotting of the deformed shape in the extended finite element analysis overlay elements can be defined. An overlay element is a 4 node linear element with a very small stiffness connected to the nodes of every enriched element and retaining the connectivity of the enriched element.

The overlay elements only have standard degrees of freedom, so their deformed shape can be visualized. The interpolation within the overlay elements is a standard bilinear interpolation, and it will not represent the discontinuities and nonlinear variation of displacements due to the enrichment functions. For the same

reason and the small stiffness of the overlay elements, the stress and strain field plots within the overlay elements do not represent the correct fields.

3.2.3 Element Crack Closure Method

When modelling complex states of loads, interaction between the crack faces may be present. For example, for some load steps, fretting fatigue can present crack closure, which can generate adhesion or frictional displacement between the crack faces.

In the standard XFEM the crack closure is not correctly modeled, so for some load stages, interference between the elements can be found as shown in Figure 16.

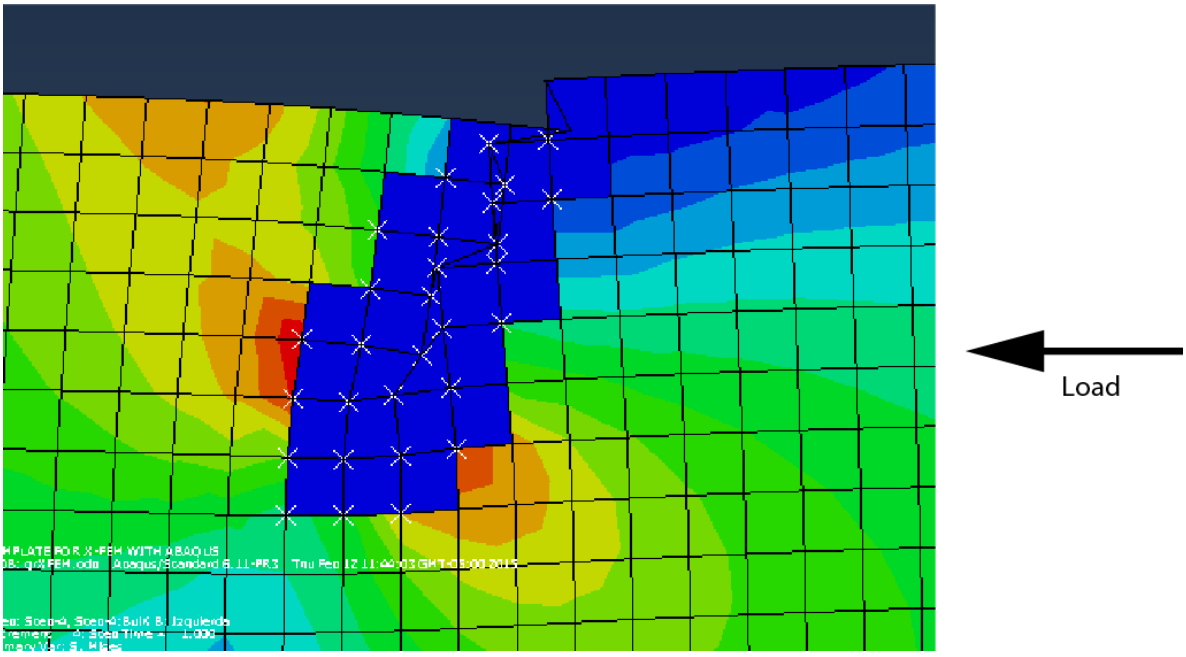

Figure 16. Standard XFEM crack closure

Multiple criteria have been developed to model crack closure; the punctual restriction criterion implemented in XFEM by Sabsabi [55] will be used.

Sabsabi modeled the contact between faces using two nodes and 2-DOF one-dimensional truss type elements, known as T2D2 in ABAQUS. As shown in Figure 17, on each point where the crack intersects an element from the mesh two nodes will be created (for example, nodes A and P). Also on the crack front two additional nodes are placed (nodes H and I).

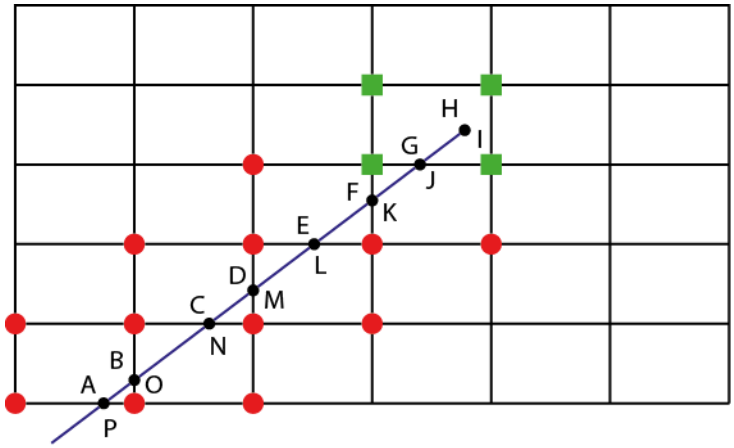

Figure 17. T2D2 node definition

The degrees of freedom of the T2D2 elements nodes are connected to the XFEM solution as a restriction; the node restriction is defined by the enrichment of the adjacent nodes. If the adjacent node has a Heaviside enrichment (as node B in Figure 17) the restriction will take the form

$$u_B = \sum_{i=1}^{2} N_i(x_B)\left[u_i + \left(H(x_B) - H(x_i)\right)a_i\right] \tag{60}$$

If the adjacent node has a crack tip enrichment (as node G in Figure 17) the restriction will have the form

$$u_G = \sum_{i=1}^{2} N_i(x_R)\left[u_i + \sum_{j=1}^{4}\left(F_j(x_G) - F_j(x_i)\right)b_i^j\right] \tag{61}$$

To guarantee that the nodes at the crack tip (nodes H and I in Figure 17) model the crack tip, an additional restriction will equal its degrees of freedom. The contact surfaces are defined by the nodes of the superior face (nodes A to H) and the inferior face (nodes I to P), assembled by T2D2 elements.

3.3 XFEM Model

The geometry to be analyzed in this work is a two dimensional complete contact fretting fatigue case, as proposed by Sabsabi [55]. A double symmetry model will be used as shown in Figure 18.

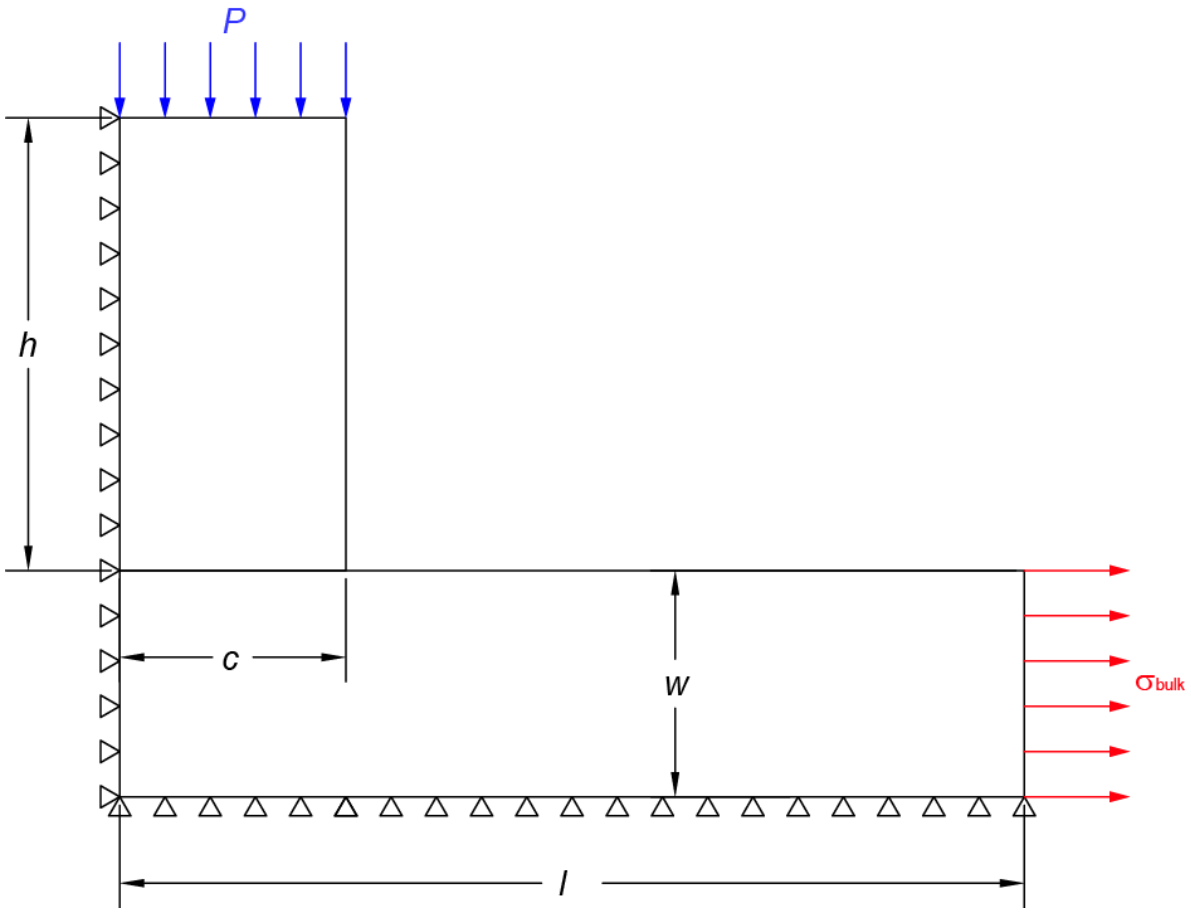

Figure 18. Model geometry.

The dimensions of the model are h = 10 mm, c = w = 5 mm, l = 20 mm and t = 1 mm, where t is the thickness of the model. Due to symmetry, the horizontal

displacement of the left nodes are restricted to zero, in the same way the inferior nodes are restrained in his vertical displacement.

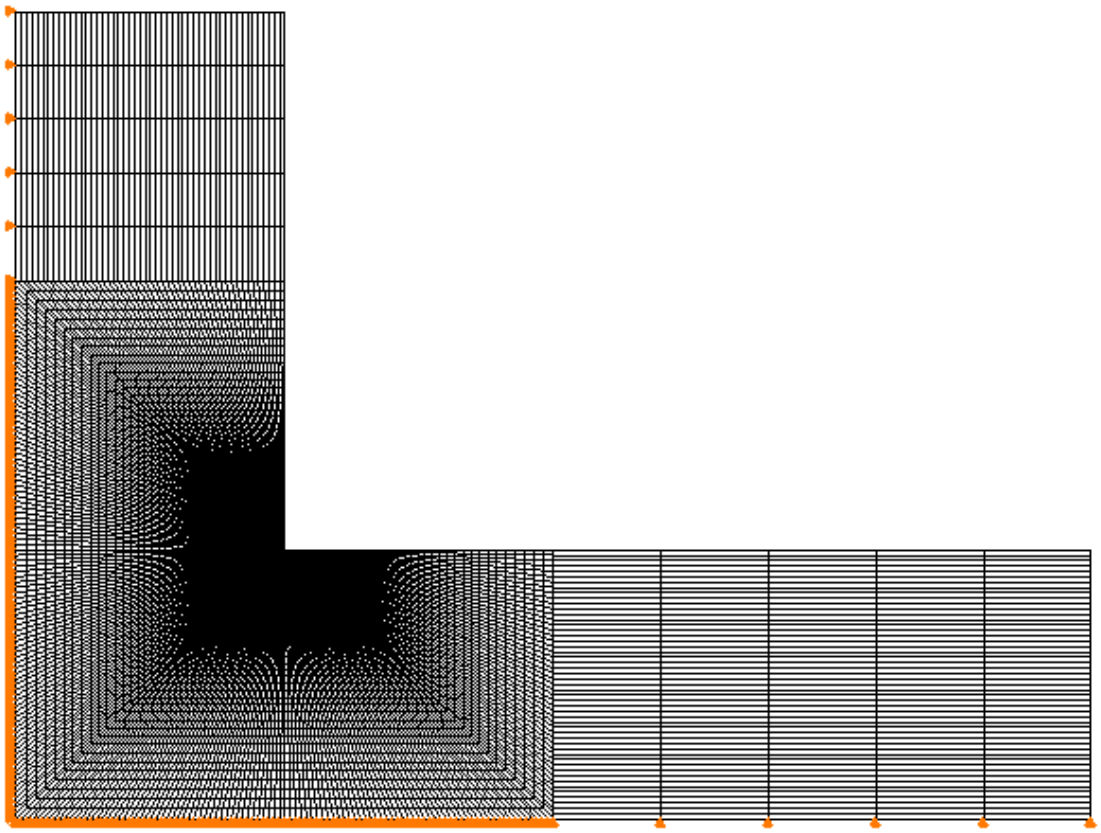

Figure 19. Model mesh representation

In Figure 19 the mesh used to solve the numerical model is shown. The orange rectangles are the restrictions imposed to the nodes due to symmetry; only linear quadrilateral elements are used. Figure 20 is a close up of the mesh in the crack zone; the dimensions of the square elements in this zone is 5 µm x 5 µm.

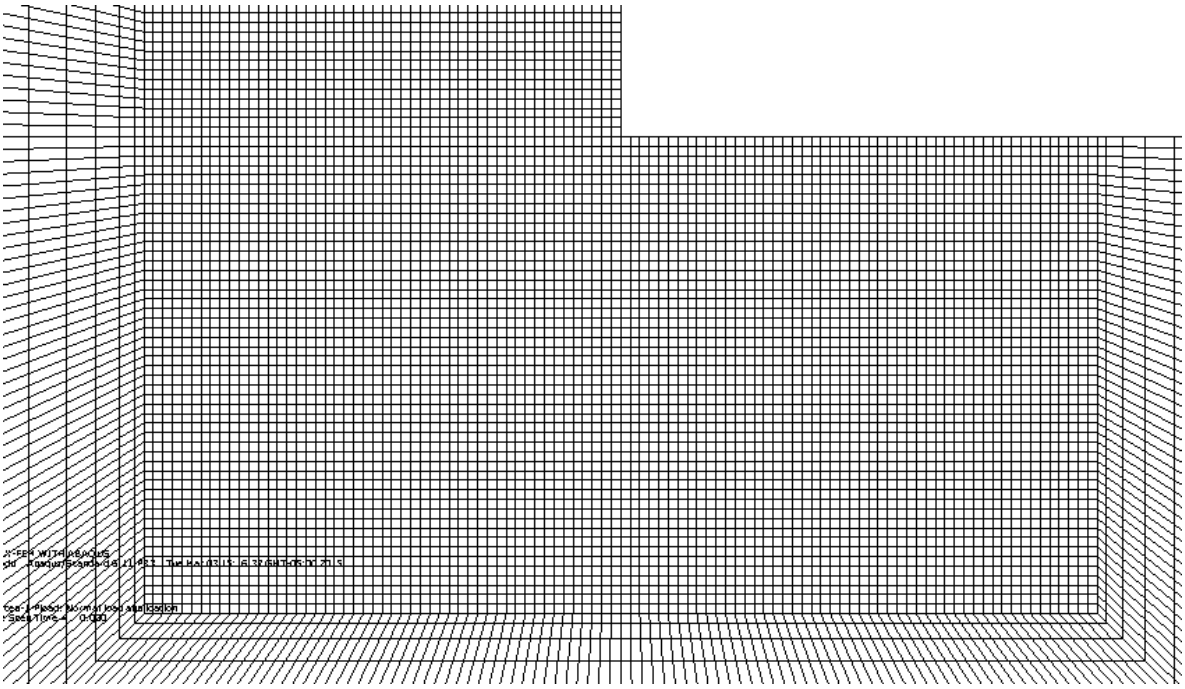

Figure 20. Model mesh zoom in crack zone

An aluminum alloy AA 7075-T6 is used for the main specimen and the indenter, the more relevant mechanical properties are shown in Table 1.

Table 1. Mechanical properties AA7075-T6

Ultimate tensile strength	σ_u	572 MPa
Tensile yield strength	σ_y	503 MPa
Modulus of elasticity	E	71.7 GPa
Poisson´s ratio	ν	0.33

Taken from: Metals Handbook Volume 2 [56]

Six load steps will be considered in the model. In the first step, the normal load P is applied until it reaches its maximum P_{max} = 40 MPa. From the second up to the sixth step the cyclic load σ_{bulk} is applied as shown in Figure 21. The maximum bulk load is $\sigma_{bulk,max}$ = 110 MPa.

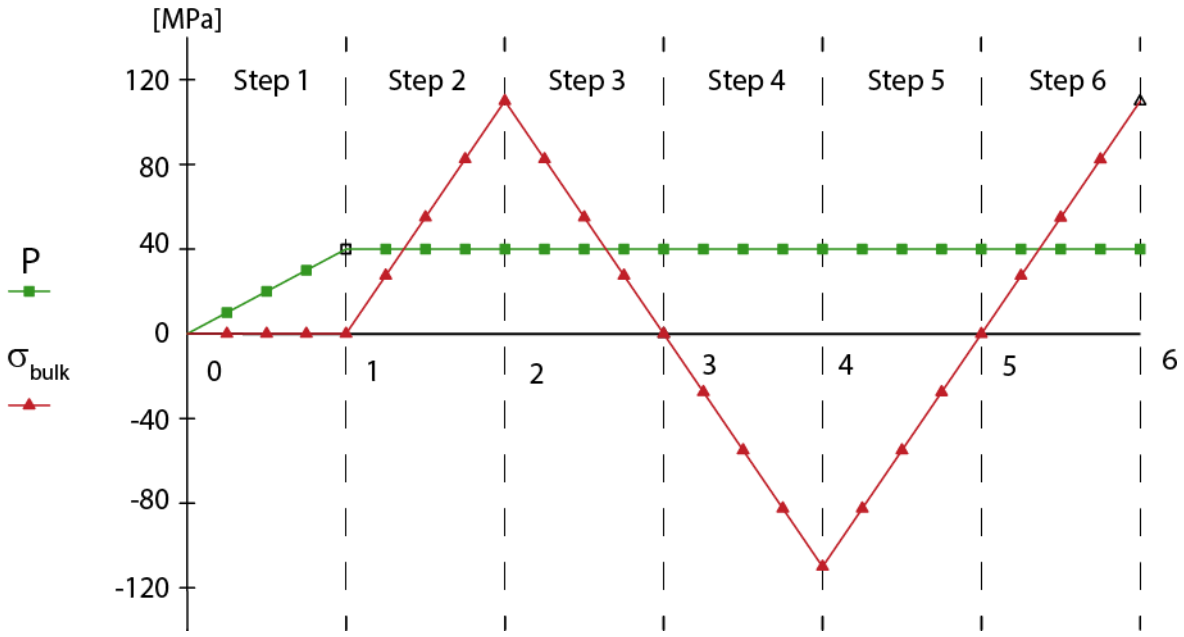

Figure 21. Applied loads in the numeric model

The initial crack direction is 60 degrees measured from the indenter contact surface with an initial length a_0 = 50 µm, the friction coefficient between all the surfaces is μ = 0.8, as proposed by Sabsabi [55].

3.4 Files Description

Implementing the XFEM in the commercial code ABAQUS imposes some restrictions, but it also provides access to the available features of the program. This section will be divided into preprocessing, processing (including a debrief of the UEL subroutine) and post-processing[1]

3.4.1 Preprocessing

The main execution file is called GenElemGG.m; in this Matlab file the geometry of the crack, the main specimen, and the indenter is read. The crack is defined as a

[1] The files description is based on Giner 2008 [52]

linear segment where the initial point is known, complemented with the initial crack length and the angle with the positive *x*-axis. The main specimen and the indenter geometries are loaded from the files m0XY.prn, m0Top.prn, miXY.prn, and miTop.prn; this is performed at the first part of the ArchivosGen.m function.

At the LevelSetMethod.m inside the ArchivosGen.m function the definition of the nodes to be enriched as a result of the crack and the mesh geometry is developed using the level set method, this is carried out by checking the sign of the scalar products of the distance vector and the normal and tangential vector to the crack.

In the remaining lines of the ArchivosGen.m function (including the Equation.m function) all the preprocessing files needed by ABAQUS are created. In Table 2 a summary of the essential files to enter the ABAQUS analysis stage is shown.

Table 2. Pre-processing input files for ABAQUS X-FEM analysis

GGnodeX	Nodes belonging to enriched elements with enrichment type and level set function values
GGinfoX	Number of crack points, number of enriched elements, number of enriched nodes
GGXYC	Coordinates of the vertices that describe the crack
GGelemX	Enriched elements with flags indicating the subdivision properties
SetNodeX2dof	Non-enriched nodes belonging to enriched elements
SetNodeX4dof	Heaviside enriched nodes
SetNodeX10dof	Crack tip enriched nodes
TopNoX	Non-enriched elements topology
TopX	Enriched elements topology
TopXoverlay	Overlay elements topology
TopT2D2	T2D2 elements topology
mT2D2	T2D2 nodes coordinates
CalEqu	T2D2 restriction nodes coefficients

3.4.2 Processing

To start the process in ABAQUS, the batch file runABQ.bat is called in Matlab. In this file the main file grXFEM.inp with the user subroutine file UEL_FEM.for is run with the ABAQUS command

```
abaqus job=grXFEM user=UEL_XFEM.for interactive
```

An ABAQUS input file is composed of a number of option blocks describing a part of the model; each option block begins with a keyword line starting with a * which is usually followed by one or more data lines. In Appendix A an example of an input file is shown.

In Section #1[2] four node user elements with 12 degrees of freedom per node are defined, they are labelled as U12. The number of properties of the element, two real value properties, and five real properties are also defined (these values are reviewed in Section #6). The number of solution state variables per element is set to a large number to be used for the output of the magnitudes at the integration points of the enriched elements (the output is defined in Section #9).

The conventional ABAQUS degrees of freedom are: DOFs 1 and 2 are the standard two dimensional displacements in the x_1, x_2 directions. DOFs 3 and 4 are intended for the x_3 displacement and the rotation about the x_1 axis, however they will be used as the Heaviside related degrees of freedom. DOFs 5 and 6 are intended for rotations about the x_2 and x_3 axes, DOF 7 for warping amplitude for open section beam elements, DOFs 11 to 15 for the first and successive temperatures in shell and beams elements. However, degrees of freedom 5-7 and 11-15 will be associated with the crack tip enrichment, DOFs 8-10 will not be used in the proposed analysis [57].

[2] The notation # is used to make reference to the section in the input file shown in Appendix A

The nodal coordinates, the topology, and the assigned material of the standard elements and the T2D2 elements are defined in Section #2. The standard elements of the main specimen are grouped into the element set ELEMTOPNOX, the elements of the indenter are grouped into the element set ELEMIDEN, and the T2D2 element are grouped in the element set ELEMT2D2.

Section #3 presents the definition of the elements set ELEMTOPXU12 including the nodes and topology of the enriched elements. In Section #4 additional node and element sets are included; these will be useful for the restriction and the loads in the model. In Section #5, the overlay elements are defined as the elements sets ElemTopXoverlay and the negligible stiffness material is assigned to it.

In Section #6, the materials definition is carried out, two materials are defined. The first one called Material-1 has the aluminum alloy properties defined in Table 1, the second one called MaterOverlay is a negligible stiffness material used for overlay and T2D2 elements. The properties of the user defined elements are defined, the first two real properties are the Young´s modulus E and the Poisson's ratio ν, the next five integer properties are a flag indicating plane stress or plain stress, the number of integration points in the enriched elements (for non-subdivided, triangular subdivided and quadrilateral subdivided elements) and the dimension of the physical domain of the problem.

In Section #7 the boundary conditions are introduced; in this section the restriction of the non-used degrees of freedom in the enriched elements defined in the elements set SetNodeX2dof, SetNodeX4dof, and SetNodeX10dof is performed. The punctual restriction between the T2D2 nodes is also defined, using the *Equation keyword and the coefficients defined in the CalEqu file.

In Section #8 the analysis procedure *coupled temperature-displacement will be used (over the standard procedure *static). Using this procedure ABAQUS will

solve the DOFs 1-7 and 11-15 simultaneously (since DOF 11-15 are originally conceived for nodal temperatures).

The output settings are defined in Section #9. User elements in ABAQUS are not output to the .odb file (output data base). The solution of the enriched elements can be printed in the .dat file; however, it is useful to print the information to the binary results file .fil for further post processing.

3.4.3 User Element Definition

The user element subroutine UEL_XFEM.for constitutes the core of the implementation. The subroutine variable declaration and structure follow the ABAQUS conventions. Initially, the properties defined in Section #6 of the grXFEM.inp file are read. Next the information related to the preprocessing is read. This includes the number of cracks, crack-patch vertices, enriched nodes and elements, type of enrichment and crack-element intersection points. In Appendix B a template of the UEL_XFEM.for archive can be found.

After initializing required vector and matrices, if the element key is U12 the subroutine int2d_X is called. In this routine the location of the integrations points is defined according to the subdivision type, and the total number of integration points (gint) is computed for the current element. In the routine TipoXelemento the keys for the enrichment type associated with the elements nodes are read. Then the routine K_U12 computes the element stiffness matrix. Once ABAQUS solves the overall system of equations, the UEL subroutine is called again and the force vector and the residual force vector are calculated at the end of the current time increment. The stresses and other important magnitudes are computed at the Gauss points and stored for output to the results file .fil in the routine SVARS_U12. In Appendix C a K_U12 subroutine template can be found.

In the subroutine K_U12, after reading the element nodal coordinates and the stress-strain constitutive matrix, a loop over the total number of integration points of the enriched element is entered. First, the standard shape functions and their derivatives are computed. Then, if the enriched elements contain Heaviside enriched nodes, the routine Heaviside is called, which returns the value of the Heaviside function in the integration points and in the nodes. Analogously, for crack-tip enriched nodes, the spatial derivatives are calculated in the routine fCrackTip, together with the nodal values for the shifted-basis enrichment. The strain-displacement element matrix **B** is then constructed and the stiffness matrix **k** is computed and returned as the ABAQUS variable AMATRX.

Before exiting the subroutine K_U12, the strain-displacement element matrix B and the Jacobian at the integration points are stored to be passed to the subroutine SVARS_U12. After solving the overall system of equations, ABAQUS calls again the user subroutine UEL in order to update the solution-dependent state variables stored in SVARS. In the subroutine SVARS_U12 strain, stress, strain energy density and strain-like magnitudes are computed at the integration points. These are stored in the array SVARS, together with the Jacobian, spatial derivatives of the shape functions N, and global coordinates of integration points. This information is needed for further post-processing of domain integrals to extract the stress intensity factors. The results are written by ABAQUS in the results binary file .fil with the label SDV as set in the input file.

3.4.4 Postprocessing

As previously mentioned, the postprocessing stage is where the information obtained from ABAQUS is processed to determine the crack propagation direction described as an angle. Two postprocessing methods will be analyzed in this work, (a) domain integrals are used to obtain the stress intensity factors and posteriorly apply the MTS criterion. (b) the stress field in front of the crack is analyzed in order to find the direction using the minimum shear stress range.

3.4.4.1 Stress intensity factor computation and MTS criterion

ABAQUS commands procedures for computing stress intensity factors through domain integrals are not applicable to the extended finite element solution, since the information generated by the user elements cannot be processed by ABAQUS. Therefore, the postprocessing of both standard and enriched elements can be performed in an external routine. The result file .fil contains all the relevant information. This file has the ABAQUS output conventions. The subroutine ABQMAIN is designed for appropriate reading of the information. This subroutine is compiled and linked through the ABAQUS execution procedure

```
abaqus make job=<subroutine file name>
```

and then run with the command

```
abaqus <subroutine file name>
```

The interaction integral described in Section 2.5.3.3 is used to compute the stress intensity factors K_I and K_{II}, following the Moes *et al.* work [40]. The q-function used in the domain integral is an annular function defined by a radius r_q measured from the crack tip; q = 1 for nodes within a circle of radius r_q and q = 0 for the rest of the nodes.

Posteriorly, the crack propagation angle is determined using the MTS criterion.

3.4.4.2 Minimum shear stress range

ABAQUS cannot report the stress field in the user defined elements; under these conditions a non enriched element in front of the crack tip must be analyzed to implement the minimum shear stress range criterion. First, the routine Stress.m is called to read the grXFEM.dat and find the average nodal stress in the analyzed element for every load step. The information obtained in the Stress.m file is used by the Angle.m routine to find the crack propagation angle. To do this, the plane stress equation transformation is used to calculate the principal stress over a loop of angles from -90° to 90°, the resultant will determine the minimum $\Delta\tau$ and the maximum $\Delta\sigma_n$and posteriorly the crack growth angle.

3.5 Summary

In this chapter, a description of the development, as well as implementation in the software ABAQUS, of the model was presented. User defined elements were used to introduced additional degrees of freedom for the elements near the crack. The shifted formulation was implemented to assure that the first two degrees of freedom were the values of physical displacements. The geometry that will be used to validate the model was described and a review of the files needed was carried out.

CHAPTER 4: RESULTS AND VALIDATION

4.1 Introduction

In this chapter a validation of the model using information from the literature is performed. Also, the model will be applied in a fretting fatigue damage analysis of a chinese railway axle.

4.2 Validation of the Model

The model under the load conditions described in Section 3.3 was implemented. Figure 22 provides the stress distribution at the end of the first step with the initial crack (see Figure 21); only the load *P* is acting in the indenter. It can be seen that the stress distribution is approximately constant in the indenter and in the zone directly under it, except for the stress concentration near the crack tip and the corner.

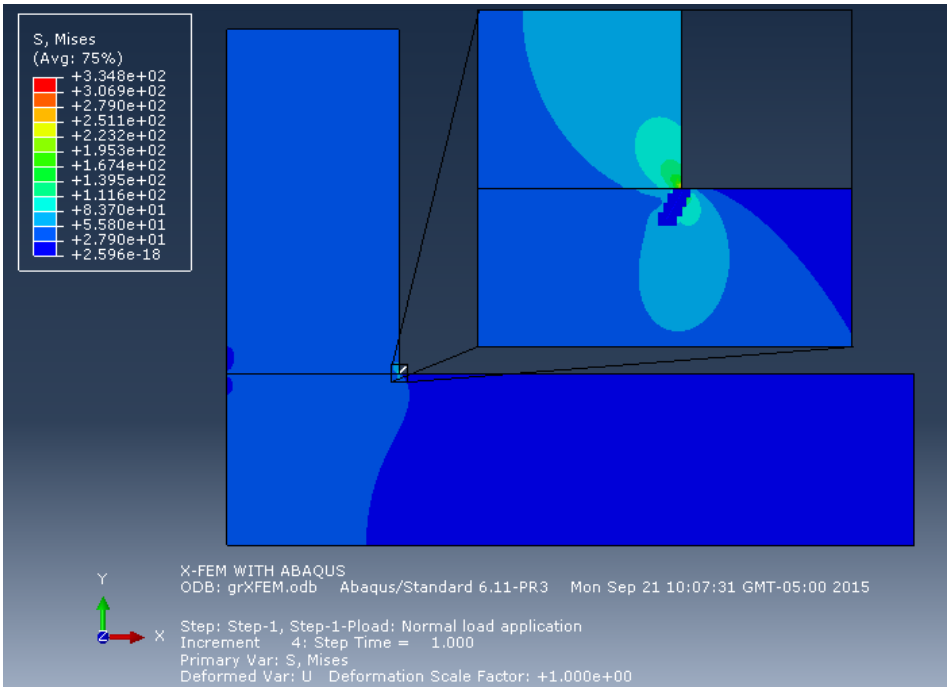

Figure 22. Initial crack stress distribution at the end of the first load step.

In Figure 23 the stress distribution at the end of the second step is shown. The bulk load is linearly increased to the right direction until it reaches it maximum. A severe stress concentration can be appreciated near the crack tip. This is expected from the introduction of the crack tip enrichment equations. At this increment, the crack must be completely open, these can be seen in Figure 24.

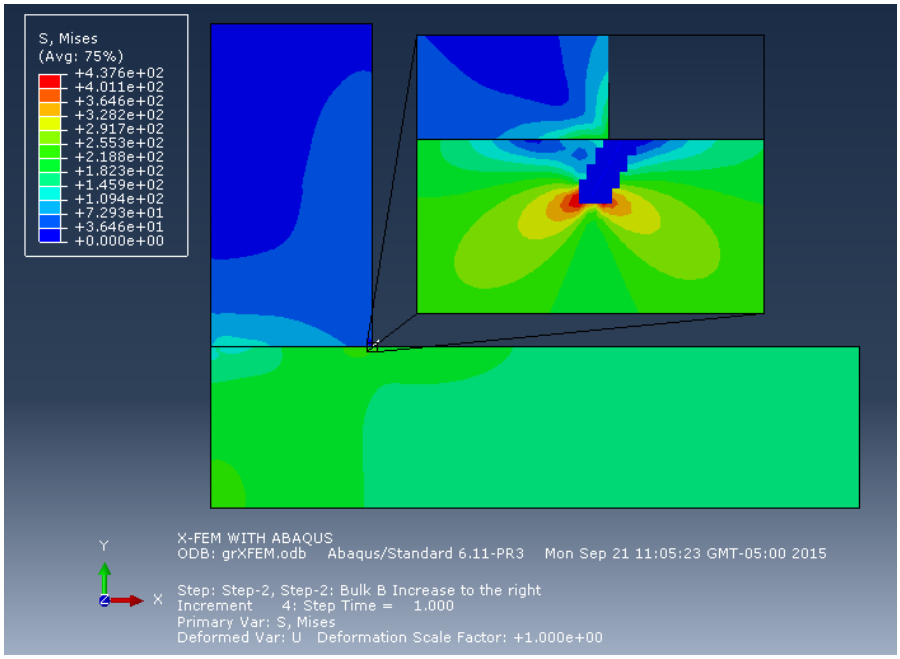

Figure 23. Initial crack stress distribution at the end of the second load step.

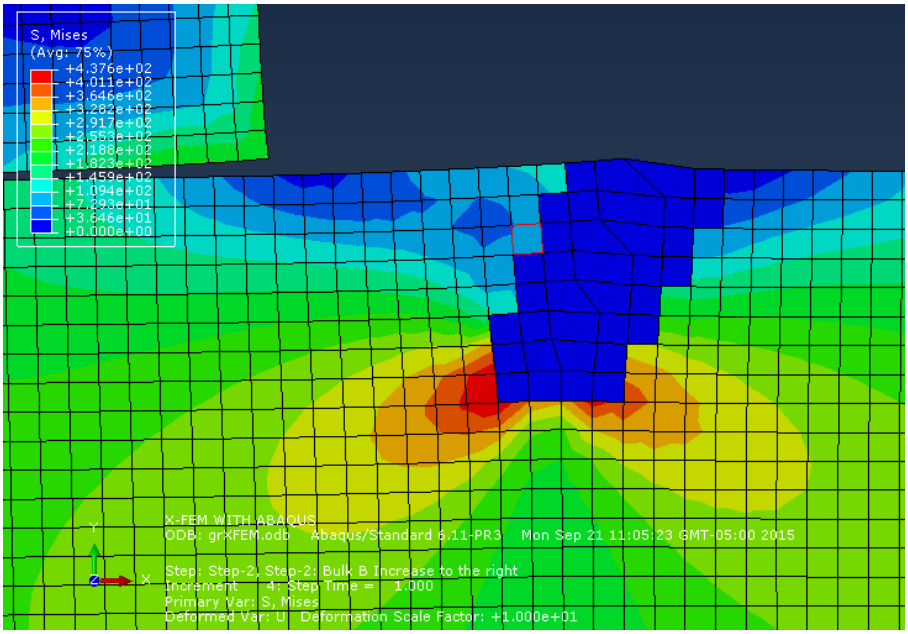

Figure 24. Near crack tip elements at the end of the second load step.

At the fourth load step, the bulk force is now applied in the left direction; the stress distribution can be found in Figure 25. In Figure 26, it can be seen that the crack is completely closed and there is no interference between the elements divided by the crack. The apparent interference between the indenter and the main specimen is just the result of the high deformation scale factor.

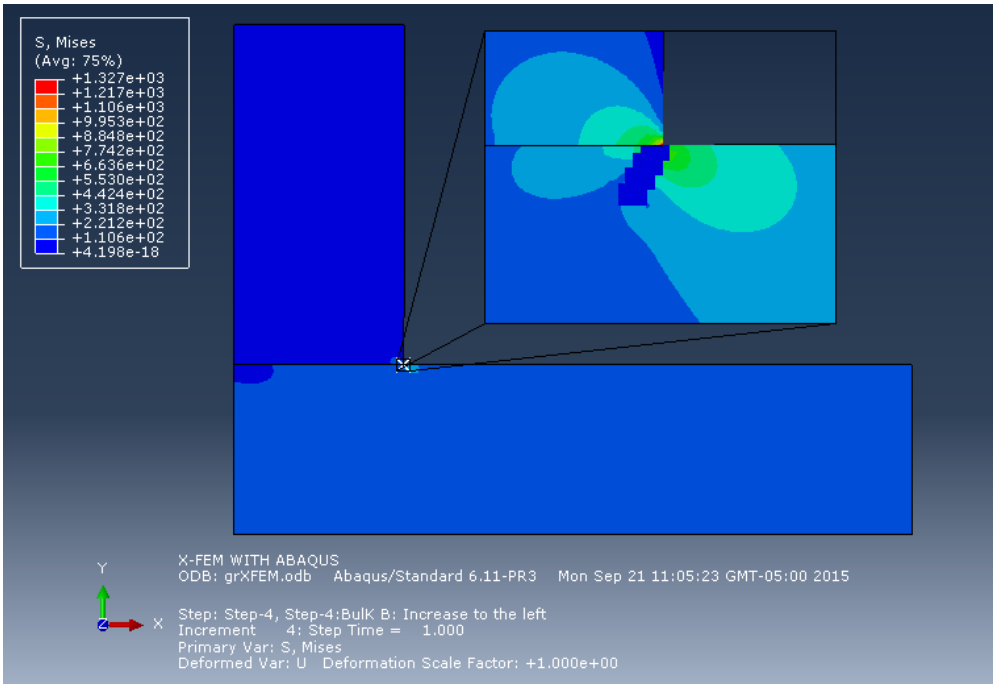

Figure 25. Initial crack stress distribution at the end of the fourth load step.

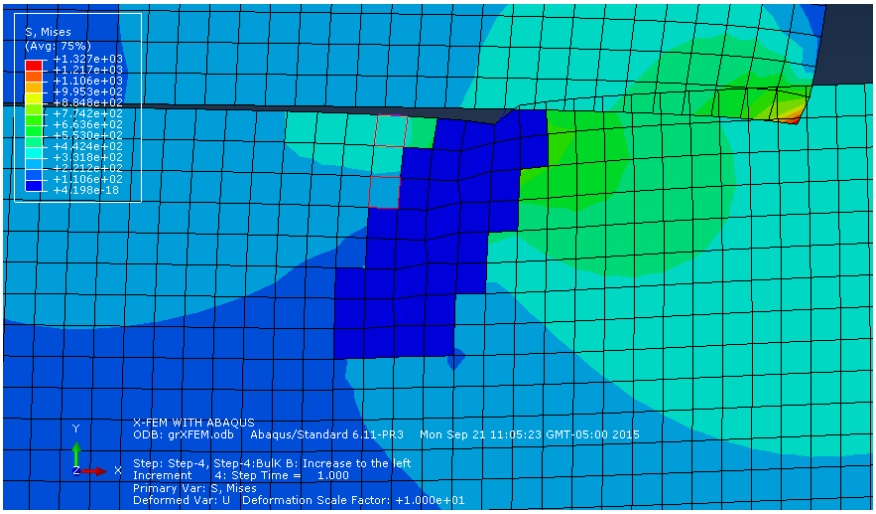

Figure 26. Near crack tip elements at the end of the fourth load step.

Finally, the model is loaded again with a force in the right direction. A stress concentration similar to the one exhibited in the second increment is found (see Figure 27). The crack is again completely open, as shown in Figure 28. At this point, the dominion integral is used to found the stress intensity factors.

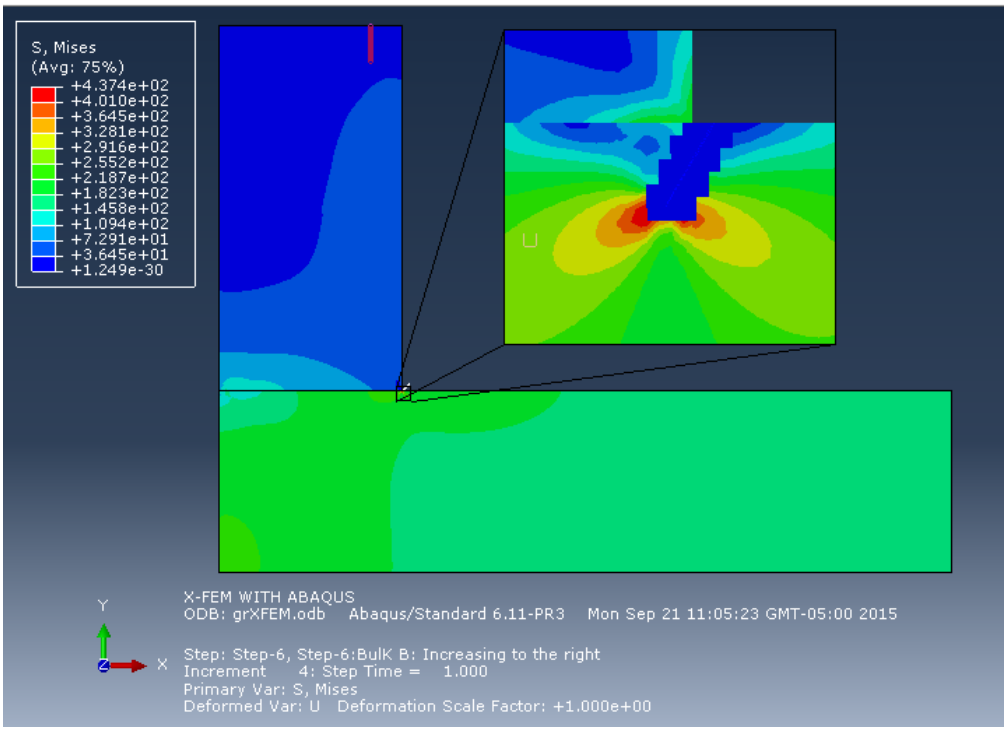

Figure 27. Initial crack stress distribution at the end of the sixth load step.

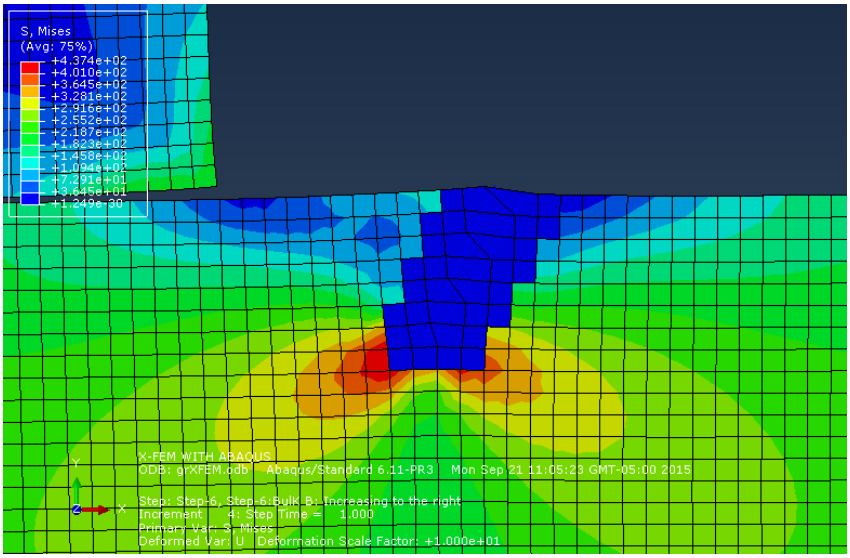

Figure 28. Near crack tip elements at the end of the sixth load step.

Figure 29 shows micrographs of fretting fatigue specimens; the tests were performed for the doctoral thesis “Modelado de grieta y estimación de vida en Fretting Fatiga mediante el Método de los Elementos Finitos Extendidos X-FEM” from the Valencia Polytechnic University. The model geometry was the described in Section 3.3 of the present work; for each micrograph the load conditions can be found in Table 3.

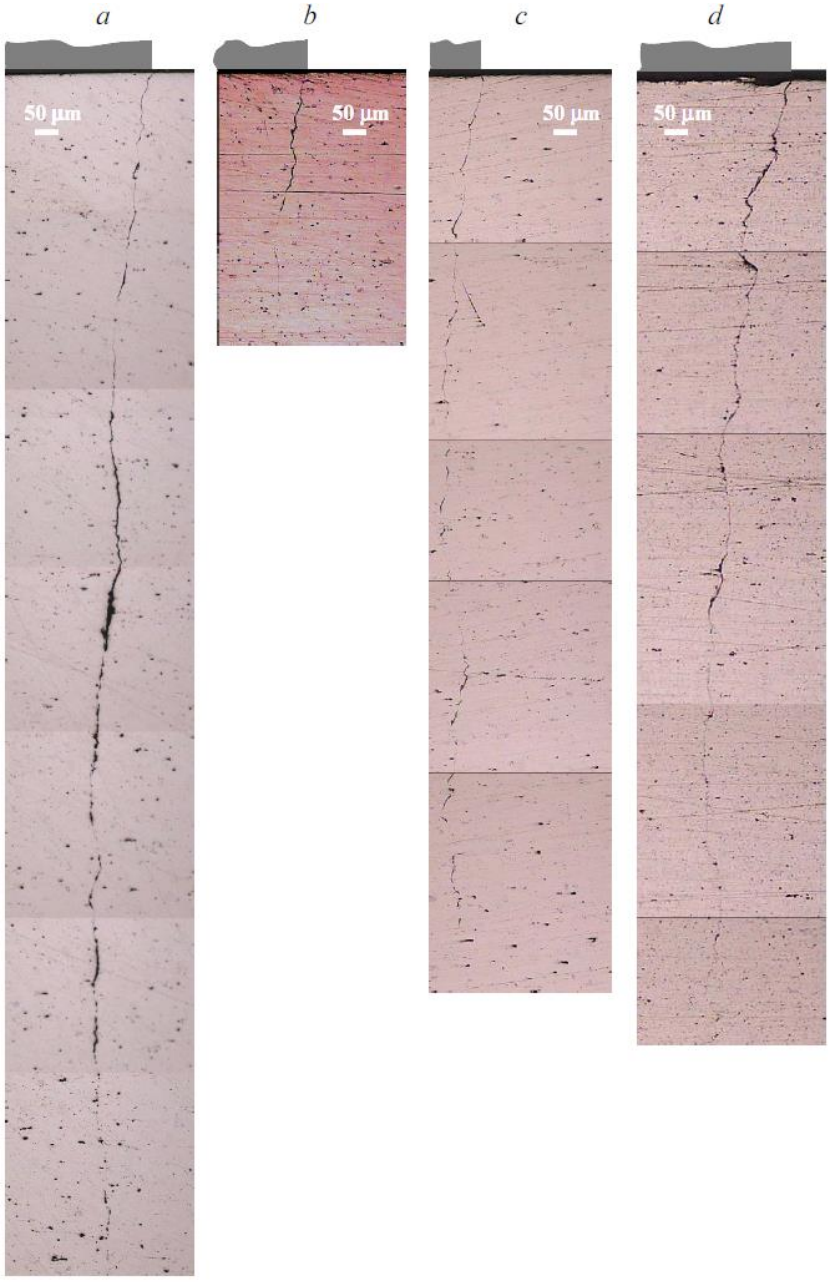

Figure 29. Fretting fatigue micrographs.

Table 3. Loads and cycles to failure.

Test	*P* [MPa]	σ_{bulk} [MPa]	*Nf* [cycles]
a	40	110	105958
b	80	130	47714
c	80	150	32905
d	160	190	8760

The maximum tangential stress criterion was implemented using the stress intensity factor, which in turn was found at the end of the sixth load step using the dominion integral. In Figure 30 the crack path predicted is shown after five increments under the load conditions in row “a” of Table 3.

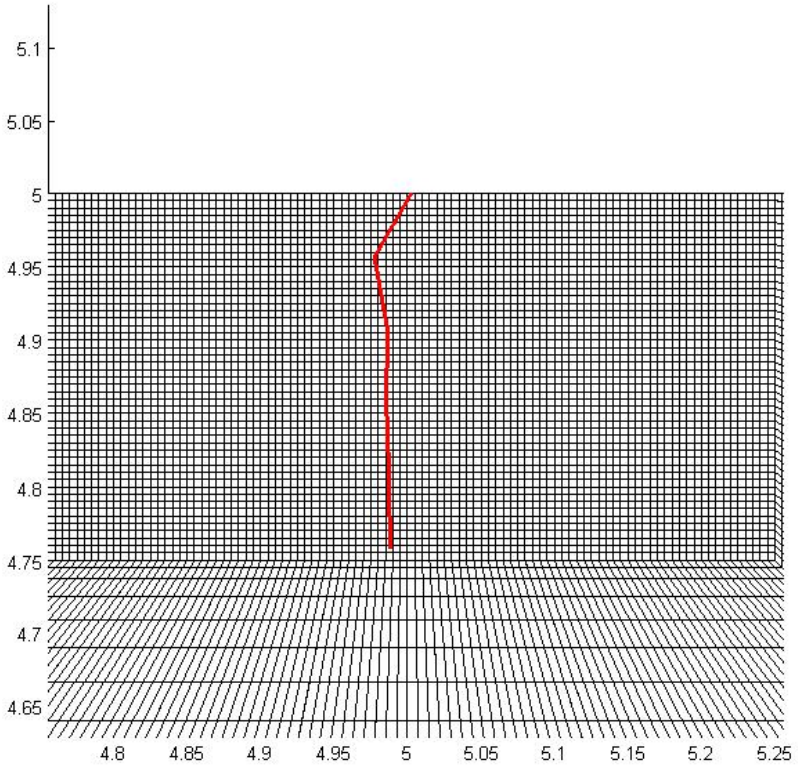

Figure 30. Predicted crack MTS criterion.

Comparing Figure 29 and Figure 30, it can be seen that the crack path is not as expected, as the crack turns prematurely to be normal to the bulk load. The error in the crack path is due to the fact that the MTS criterion only studies the stress intensity factor at the maximum bulk load step.

The crack path was also predicted using the minimum shear stress range criterion. In Figure 31 to Figure 34, the predicted crack paths under the load conditions of Table 3 can be found; all the figures present the fifth crack increment.

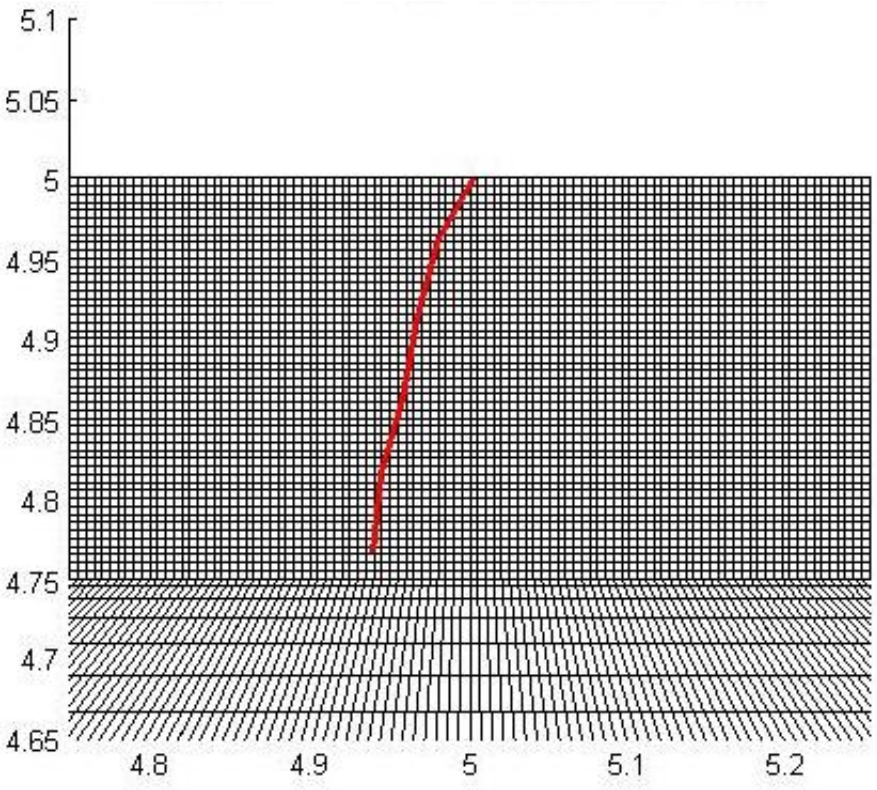

Figure 31. Crack path prediction P = 40 MPa σ_{bulk} = 110 MPa

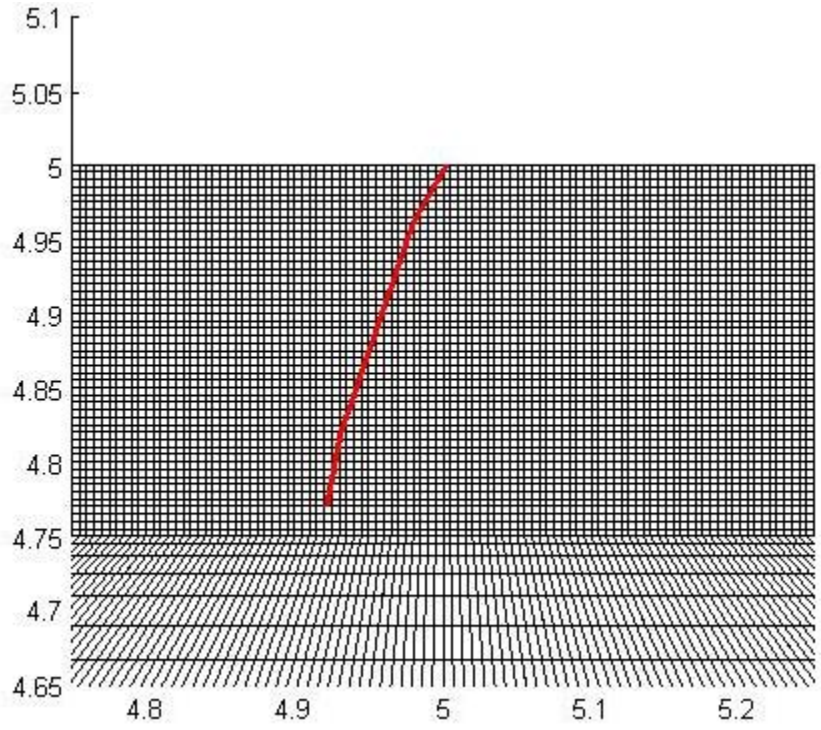

Figure 32. Crack path prediction P = 80 MPa σ_{bulk} = 130 MPa

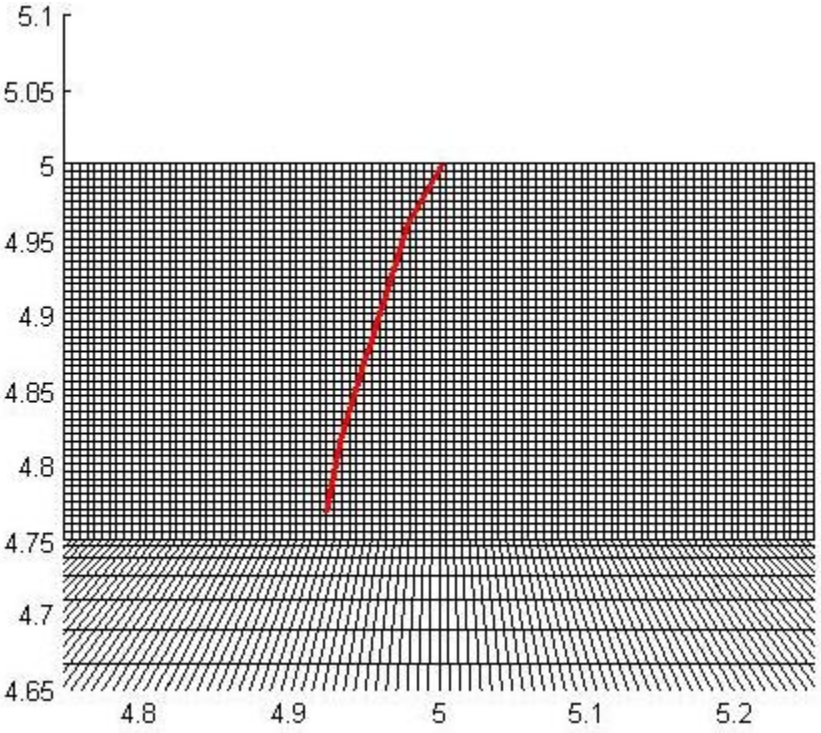

Figure 33. Crack path prediction P = 80 MPa σ_{bulk} = 150 MPa

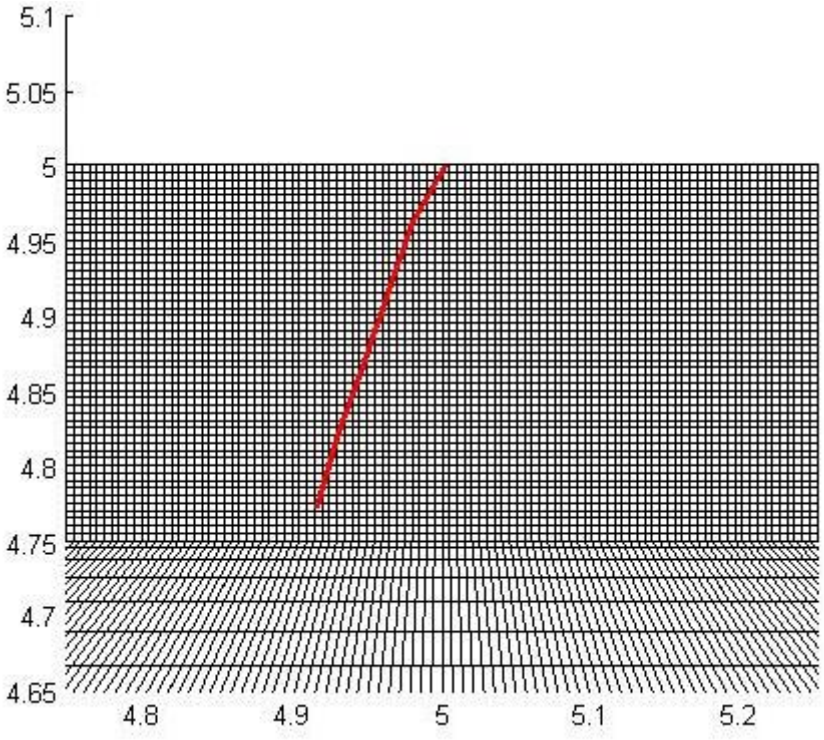

Figure 34. Crack path prediction *P* = 160 MPa σ_{bulk} = 190 MPa

The predicted crack paths using the minimum shear stress range criterion are similar to the crack paths observed in the mycrographs. Therefore, this criterion is more appropriate in this case.

4.3 Results

In Song *et al.* [58], a bending fretting fatigue damage analysis of a chinese railway axle and a simulation test of small scale wheel set were developed. In the paper, railway wheel sets with RD_2 axles were used to analyze the fretting fatigue behavior; the axles served about 20 years in situ. Also a fretting fatigue test was developed on a geometrically similar small scale railway. A conclusion in the paper was that the experimental study on small scale axle is an effective way to understand fretting fatigue damage mechanisms of real railway axles.

The small scale test developed is shown in Figure 35. A structure of press-fitted wheel-axle was used for the test. The axle specimen was mounted on the rig by a pinchcock to transmit the rotatory motion. The rotatory speed range was 0-5000 rpm controlled by an AC converter. A riven wheel was used to support the wheel and rotate with it during the test. A high speed bearing was used to apply the bending load to the specimen, the load was generated by a dead weight through a lever system which is not shown.

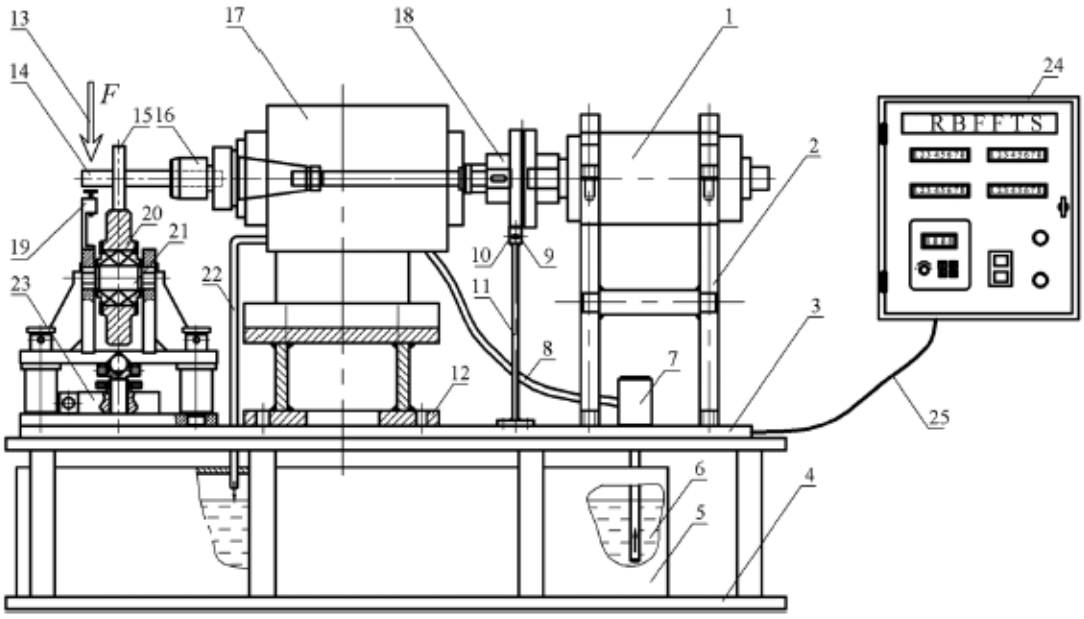

Figure 35. Rotatory bending test rig. 1-motor, 2-bracket for motor, 3-surface plate, 4-base, 5,6,7,8,22-oil refrigeration system, 9,10,11-tachometer system, 13-loaing force, 14-axle specimen, 15-half wheel set specimen, 16-pinchcook, 17-heastcock, 18-principal axle, 19-coupling, 20-driven wheel, 21-riven shaft, 23-pressure sensor, 24-control chamber and 25-cable

Adapted from: Song *et al.* [58]

In Figure 36 the dimensions of the small scale railway axle are shown. The degree of interference between the axle and the hub was set as 15 μm, the main mechanical properties of the axle and the hub can be found in Table 4.

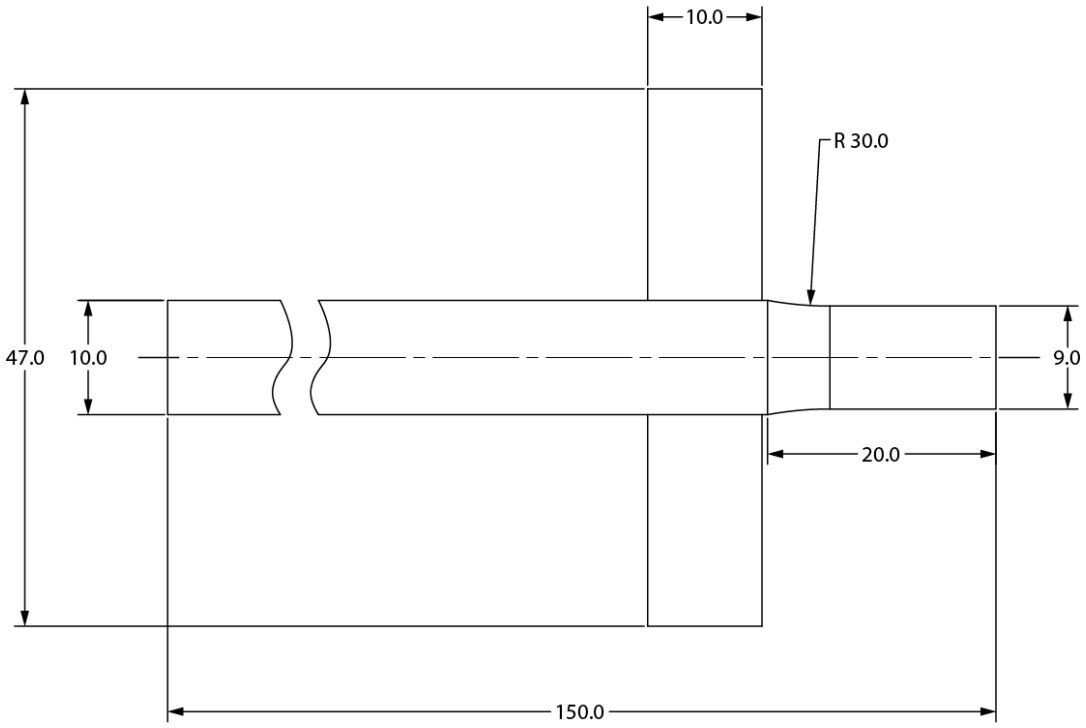

Figure 36. Test axle and wheel dimensions.

Table 4. Main mechanical properties of test axle and wheel materials

Steels	σ_s **(MPa)**	σ_b **(MPa)**	HV_{50g}	E **(GPa)**
LZ50-axle	330	650	245	210
CL60-wheel	400	820	290	210

Figure 37 diplays scanning electron micrographs of the freeting fatigue observed at the real axle (a) and the small-scale axle (b) after 4.5 x 10^6 cycles. The small-scale axle exhibited a fretting fatigue crack that inittiates about 1 mm away from the inner shrink rim; the small-scale axle specimen was under a bending stress of 144 MPa.

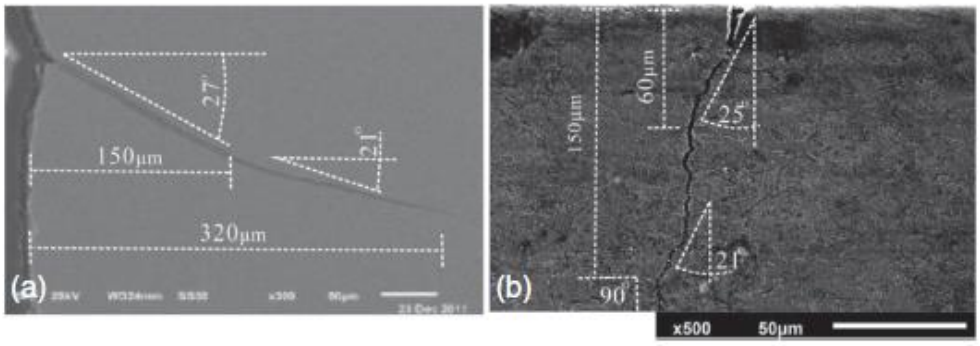

Figure 37. Scanning electron microscope image of fretting fatigue crack observed.

Adapted from: Song et al. **[58]**

The model developed in this work was implemented to the geometry described by Song *et al.* [58]. A simple symmetry model was used. In Figure 38, the geometry, restrictions, and loads of the model are shown. The horizontal displacements of the left nodes are restricted to zero. In the same way the inferior nodes of the wheel are restrained in his vertical displacement. The distance between the right face of the wheel and the point where the shaft start reducing its diameter is set at 5 mm (there is no information about that dimension in the article).

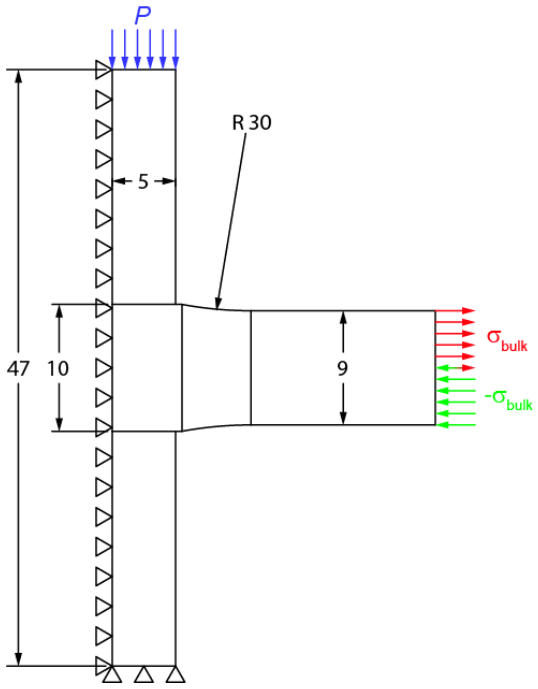

Figure 38. Axle and wheel model geometry

In Figure 39 a close up of the mesh near the crack zone is shown, the dimensions of the smallest square elements is 10 μm x 10 μm. The initial crack direction is 65 degrees measured from the contact surface with an initial length a_0 = 60 μm, crack increments of 30 μm were defined, and the friction coefficient between all the surfaces is set at μ = 0.7

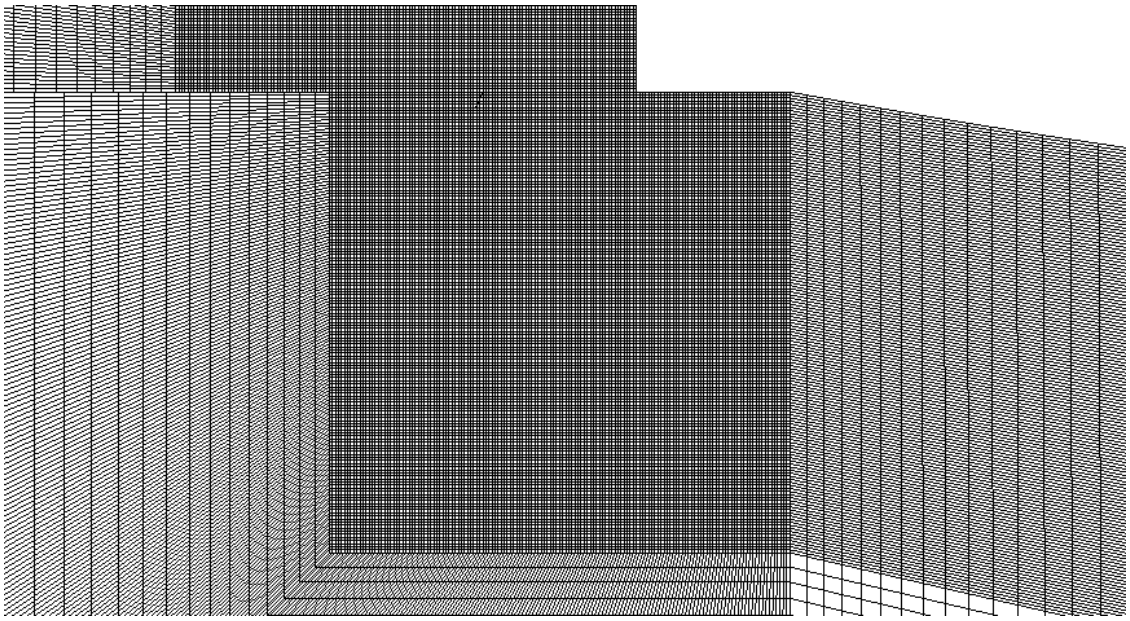

Figure 39. Axle and wheel model mesh zoom in crack zone

The *P* load simulates the contact pressure between the axle and the wheel. According to Song *et al.* [58], using the Lame's contact pressure foundation, it is approximately 150 MPa. The σ_{bulk} is placed to simulate the bending stress in the axle, a 144 MPa bending stress is required. Using the normal stress for beam loaded in bending the maximum value for σ_{bulk} is 96 MPa.

Six load steps will be considered in the model. In the first step the normal load *P* is applied until it reaches its maximum P_{max} = 150 MPa. From the second until the sixth step the cyclic load σ_{bulk} is applied, as shown in Figure 40, where the maximum bulk load is $\sigma_{bulk,max}$ = 96 MPa.

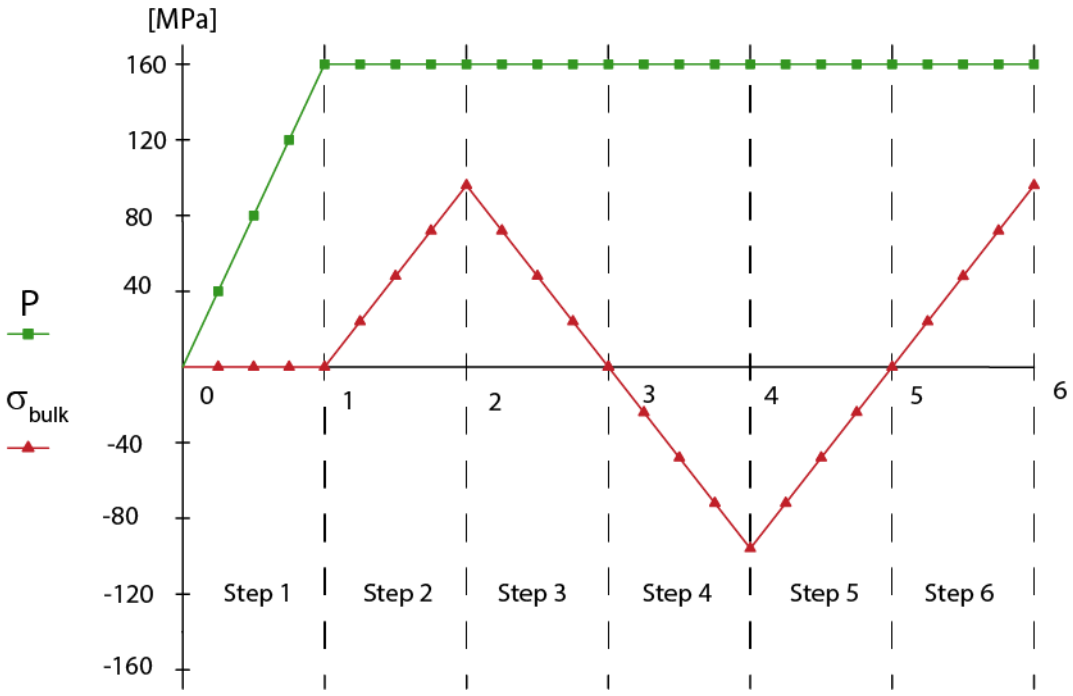

Figure 40. Applied loads in the axle and wheel model

Figure 41 shows the resultant stress distribution at the end of the first step with the initial crack; only the normal load *P* is acting in the indenter. The stress concentration at the end of the contact between the axle and the wheel can be observed.

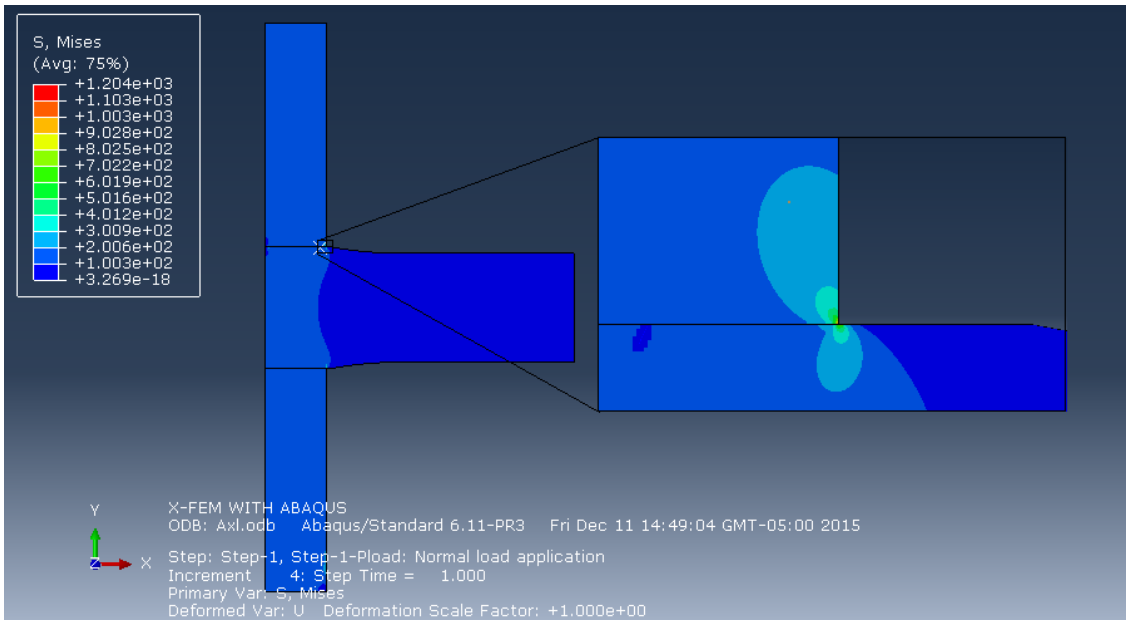

Figure 41. Initial crack stress distribution at the end of the first load step, axle and wheel model

In Figure 42 and Figure 43 the initial crack stress distributions at the end of the second and sixths step are shown. The bulk loads are linearly increased until the negative moment reaches its maximum. The crack tip stress concentration could not be appreciated due to the high normal load and the resultant stress concentration at the end of the contact.

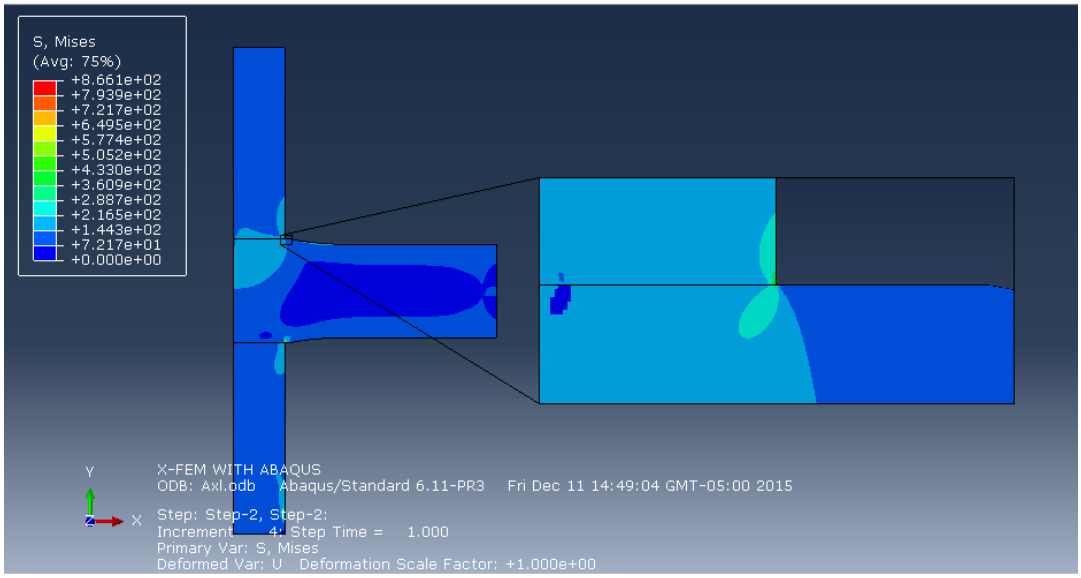

Figure 42. Initial crack stress distribution at the end of the second load step, axle and wheel model

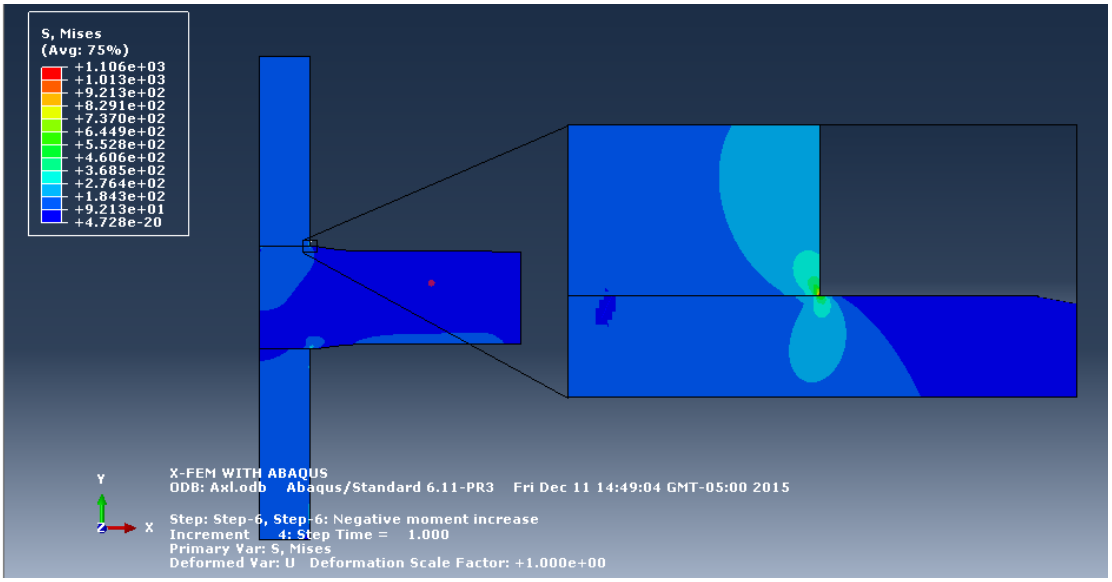

Figure 43. Initial crack stress distribution at the end of the sixth load step, axle and wheel model

The predicted crack path at the fifth increment under the described conditions can be found in Figure 44.

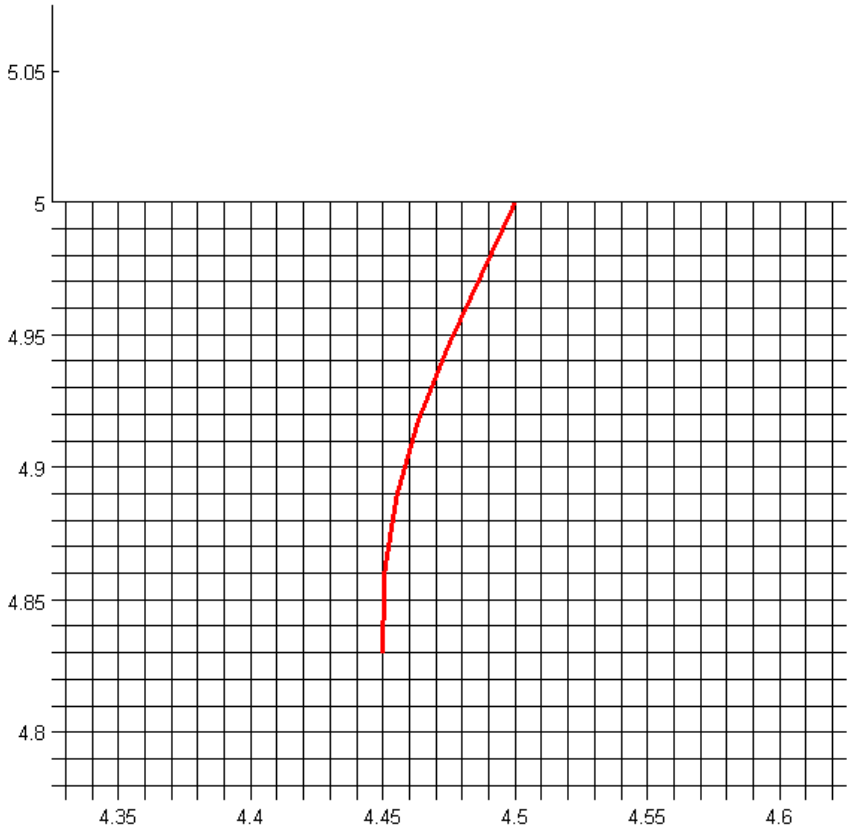

Figure 44. Crack path prediction, axle and wheel model

In Figure 45, a superposition of the predicted crack path and the Song *et al.* [58] micrograph can be found. The predicted and the real cracks have similar paths. Although the real crack has a higher inclination at early stages, as the crack grows both crack paths become similar. It can be concluded that the crack path found is an acceptable approximation for the real crack.

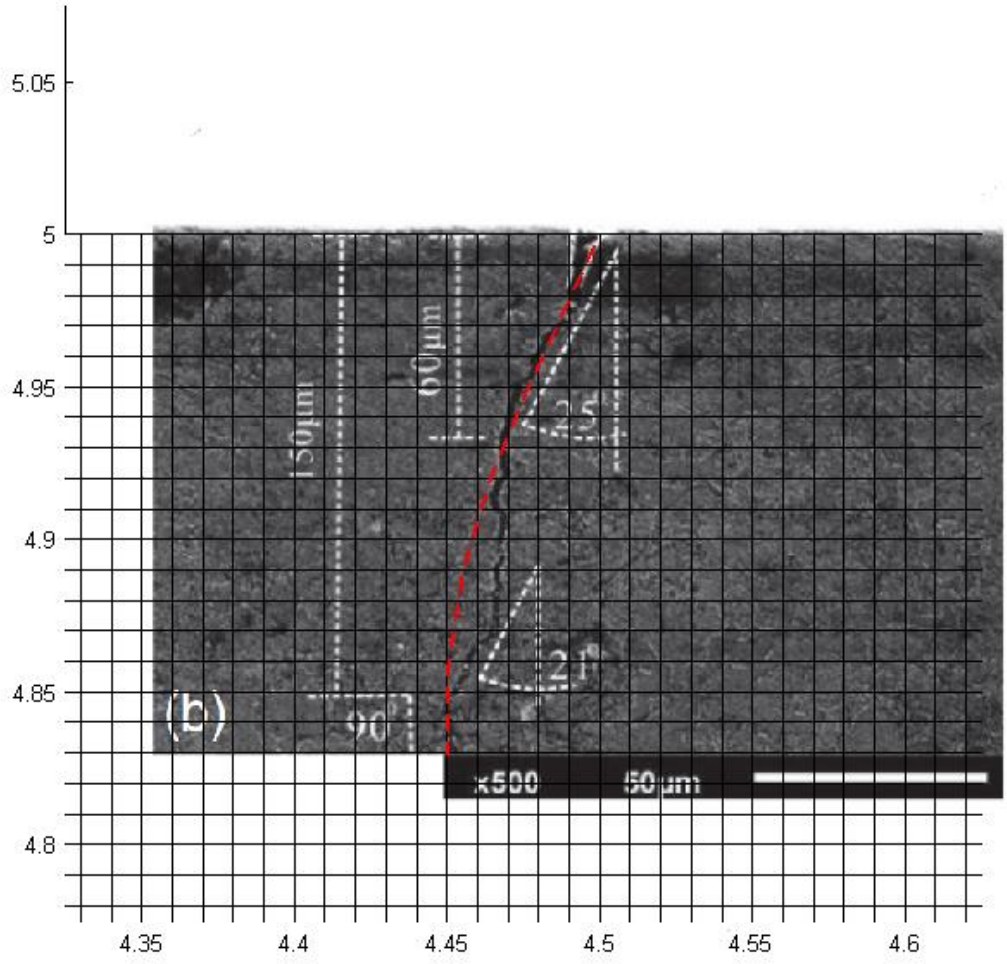

Figure 45. Crack path prediction - real crack micrograph superposition

CHAPTER 5: CONCLUSIONS AND FURTHER WORKS

5.1 Conclusions

In this work, an Extended Finite Element Model (XFEM) of fretting fatigue crack growth was developed. The crack paths for two fretting fatigue configurations were predicted. During the development of the model, the following achievements were obtained:

- A literature review of fracture mechanics and fretting fatigue was carried out, and the theories necessary for crack path prediction were studied. Crack initiation dynamics was studied, but it was not implemented in the model. An average crack initiation length and inclination were selected from the literature. The maximum tangential stress and the minimum shear stress range criteria were selected to predict the crack path direction.

- The theory of the Finite Element Method (FEM) was studied, and the XFEM method was selected to be implemented in the model, a shifted enrichment formulation was employed to define the contribution of the standard degrees of freedom plus the enriched contribution. Also, the domain integrals to calculate the stress intensity factor were studied.

- The XFEM method was implemented using the software Matlab and ABAQUS. A punctual restriction criterion using T2D2 ABAQUS elements was used to simulate crack closure. The stress intensity factors were found using interaction integral method implemented in FORTRAN.

- The model was validated with the results of similar works developed by researches in the field. The predicted crack using the Maximum Tangential Stress criterion was not similar to the validation information, and it was not implemented in the final model. The predicted crack using the minimum

shear stress range criterion compared to the validation information shows acceptable results.

- The model was implemented using data from Chinese railway small scale fretting fatigue test. Although the real crack has a higher inclination at early stages, as the crack grows both crack paths become similar, and it could be concluded that the crack path predicted was an acceptable approximation for the real test crack.

- This work has shown that is possible to predict the crack path in elements under fretting fatigue. It is an important step to create a more accurate fracture model. A more accurate solution can be used to take decisions in critical life extension problems. Also, it can be used to provide valuable information for the design of elements prone to fatigue failure.

5.2 Further works

As a result of the work developed in this thesis, several research directions are foreseen, as some issues were not dealt with in the current work.

- Extension of the current model to include a previous analysis of the initiation phase.

- Analysis of the possible implementation of a segment-to-segment crack closure model and compare it to the current model.

- Analysis of the implementation of transition elements and compare the results with the current model.

- Development of a similar XFEM model that is able to work with 2D triangular elements and 3D hexahedral elements.

- Application of the results of the current model to a more complete life time prediction model.

- Application of similar enrichment functions to study cases susceptible to local discontinuities.

- Analysis of the results of the model for different load conditions.

CHAPTER 6. REFERENCES

[1] A. S. Balankin, Mecánica de la Fractura: Pasado, Presente y Futuro. Memorias del Quinto Congreso Nacional de Ingeniería Electromecánica y de sistemas., Mexico DF, 2000, pp. 313-328.

[2] A. Griffith, "The Phenomenon of Rupture and Flow in Solids.," *Philosophical Transaction of the Royal Society of London,* vol. 221, pp. 163-198, 1920.

[3] I. V. Obreimoff, "The Spliting Strenght of Mica," *Proceeding of the Royal Society of London,* 1930.

[4] G. P. Cherepanov, Brittle Fracture Mechanics, New York: McGraw Hill, 1978.

[5] A. S. Balankin, Kinetic Theory of Strenght and Fracture., Moscow: Ministry of Defense USSR, 1990.

[6] A. S. Panasyuk, Material Quasi-Brittle Fracture, Kiev: Naukova DUmka, 1991.

[7] G. R. Irwin, "Analysis of Stresses and Strains Near the End of a Crack Traversing a Plate," *9th International Congress in Applied Mechanincs,* pp. 361-364, 1957.

[8] M. L. Williams, "On the Stress Distribution on the Base of a Stacionary Crack," *Journal of Applied Mechanical.,* pp. 109-114, 1957.

[9] G. R. Irwin, "Fracture, Encyclopedia of Physics, Elasticity and Plasticity," 1958. [Online].

[10] D. A. Hills and D. Nowell, "Mechanics of Fretting Fatigue," *Solid Mechanics and its Applications,* 1994.

[11] P. L. Hurricks, "Mechanism of wearing," *Wear,* no. 15, pp. 397-407, 1970.

[12] K. Nishioka and K. Hirakawa, "Fundamental Investigations of Fretting Fatigue," *Bulletin of JSME,* Vols. 397-407, no. 12, 1969.

[13] K. Endo and H. Goto, "Initiation and propagation of fretting fatigue cracks," *Wear,* no. 38, pp. 311-324, 1976.

[14] M. P. Szolwinski and T. N. Farris, "Mechanics of Fretting Fatigue Crack Formation," *Wear,* no. 198, pp. 93-107, 1996.

[15] R. D. Mindlin, "Compliance of Elastic Bodies in Contact," *Journal of Applied Mechanics,* vol. 16, pp. 259-268, 1949.

[16] U. Bruggman and S. Soderberg, "Contact conditions on fretting," *Wear,* no. 110, pp. 1-17, 1986.

[17] J. Juoksukangas and A. Lehtovaara, "The effect of contact edge geometry on fretting fatigue behavior in complete contacts," *Wear ,* no. 308, pp. 206-212, 2013.

[18] I. G. Goryacheva and H. Murthy, "Contact problem with partial slip for the inclined punch with rounded edges," *International Jouranl of Fatigue,* no. 24, pp. 1191-1201, 2002.

[19] A. Sackfield and C. Truman, "The tilted punch under normal and shear load (with application to fretting tests)," *International Journal of Mechanical Sciences,* vol. 43, pp. 1881-1892, 2001.

[20] E. Popova and V. L. Popova, "The research works of Coulomb and Amontons and generalized laws of friction," *Friction,* vol. 3, no. 2, June 2015.

[21] J. O. Smith and C. K. Liu, "Stresses Due to Tangencial and Normal Loads on a Elastic Solid with Application to Some Contact Stress Problem," *Journal of Applied Mechanics,* no. 20, 1953.

[22] E. I. Radzimosky, "Stress Distribution and Strength Conditions of Two Rolling Cylinders Pressed Together," *University of Illinois Engineering Experimental Station,* 1953.

[23] D. L. McDiarmid, A General Criterion for High Cycle Multiaxial Fatigue Failure, London: Department of Mechanical Engineering and Aeronautics, 1990.

[24] M. W. Brown and K. J. Miller, "A Theory for Faitgue Under Multiaxial Stress-Strain conditions," *Proceedings of the Institution of Mechanical Engineer,* no. 187, 1973.

[25] A. Fatemi and D. F. Socie, A Critical Plane Approach to Multiaxial Fatigue Damage Incluiding Out-of-Phase Loading, Illinois, 1987.

[26] R. Smith, P. Watson and T. Topper, "A Stress Strain Function for the Fatigue

of Metals," *Journal of Materials JMLSA,* pp. 767-778, 1970.

[27] B. Crossland, "Effect of Large Hidrostatic Pressures on the Torsional Fatigue Strenght of an Alloy Steel.," *Proceedings International Conference on Fatigue of Metals.,* pp. 138-149, 1956.

[28] F. Erdogan. and G. C. Sih, "On the Crack Extension in Plates Under Plane Loading and Tranverse Shear," *Journal of Basic Engineering,* vol. 85, no. 4, pp. 519-525, 1963.

[29] R. J. Nuismer, "An Energy Release Rate Criterion for Mixed Mode Fracture," *International Journal of Fracture,* vol. 11, no. 2, 1975.

[30] M. A. Hussain, S. L. Pu and J. Underwood, "Strain Energy Release Rate for a Crack Under Combined Mode I and Mode II," 1974.

[31] G. Sih, "Strain-Energy-Density Factor Applied to Mixed Mode Crack Problems," *International Journal of Fracture,* vol. 10, no. 3, 1974.

[32] B. Cotterell and J. R. Rice, "Slightly curved or kinked cracks," *Internation Journal of Fracture,* vol. 16, no. 2, pp. 155-169, 1980.

[33] E. Giner, M. Sabsabi, J. J. Ródenas and F. Fuenmayor, "Direction of Crack Propagation in a Complete Contact Fretting-Fatigue," *International Journey of Fatigue,* vol. 58, pp. 172-180, 2014.

[34] R. Courant, "Variational Method for the Solution of Problems of Equilibrium and Vibrations," *Bulletin of the American Mathematical Society,* vol. 49, no. 1, 1943.

[35] S. S. Quek and G. R. Liu, Finite Element Method: A Practical Course, Butterworth-Heinemann, 2003.

[36] C. Fernández Cueto, Análisis por MEF del Comportamiento Mecánico de Grietas Internas en la Región Metal Base-Zac-Metal Depositado de Soldadura SAW en Tubo API 5L X52, Mexico D.F.: Instituto Politécnico Nacional, Escuela Superior de Ingeniería Química e Industrias Extractivas, 2010.

[37] T.-P. Fries, "The Extended Finite Element Method," RWTH Aachen University, [Online]. Available: http://www.xfem.rwth-aachen.de/. [Accessed 2 11 2014].

[38] S. Osher and J. Sethian, "Fronts Propagating with Curvature Dependent Speed: Algorithms Based on Hamilton-Jacobi Formulations," *Computational Physics,* vol. 79, 1988.

[39] T. Belytschko and T. Black, "Elastic crack growth in finite elements with minimal remeshing," *International Journal for Numerical Methods in Engineering,* vol. 45, no. 5, june 1999.

[40] N. Moës, J. Dolbow and T. Belytschko, "A Finite Element Method for Crack Growth Without Remeshing," *International Journal for Numerical Methods in Engineering ,* vol. 46, no. 1, 1999.

[41] G. Zi and T. Belytschko, "New crack-tip elements for XFEM and applications to cohesive cracks," *International Journal for Numerical Methos in Engineering,* vol. 57, no. 15, pp. 2221-2240, 2003.

[42] H. Bueckner, "A novel principle for the computation of stress intensity factor," *Zeitschrift fuer Angewandte Mathematik & Mechanik,* vol. 50, no. 9, 1970.

[43] J. R. Rice, "Some remarks on elastic crack-tip stress field," *International Journal of Solids and Structures,* vol. 8, no. 6, 1972.

[44] S. K. Chan, I. S. Tuba and W. K. Wilson, "On the finite element method in linear fracture mechanics," *Engineering Fracture Mechanics,* vol. 2, no. 1, 1970.

[45] D. R. J. Owen and A. Fawkes, Engineering Fracture Mechanics: Numerical Methods and Applications, Swansea, UK: Pineridge Press Ltd, 1983.

[46] S. L. Pu, M. A. Hussain and W. E. Lorensen, "The Collapsed cubic isoparametric element as a singular element fro crack problems," *International Journal for Numerical Methods in Engineering,* vol. 12, no. 11, 1978.

[47] S. H. Ju, "Simulating three-dimensional stress intensity factors by the least-squares method," *International Journal for Numerical Methods on engineering,* vol. 43, no. 8, 1998.

[48] J. D. Eshelby, "The Energy Momentum Tensor in Continuum Mechanics," in *Fundamental Contributions to the Continuum Theory of Evolving Phase*

Interface in Solids, Springer Berlin Heidelberg, 1970.

[49] J. R. Rice, "A path independent integral and the approximate analysis of strain concentration by notches and cracks," *Journal of Applied Mechanics,* no. 35, 1968.

[50] T. K. Hellen and W. S. Blackburn, "The calculation of stress intensity factor for combined tensile and shear loading," *International Journal of Fracture,* vol. 11, no. 4, 1975.

[51] F. Z. Li, A. Shih and A. Needleman, "A comparison of methods for calculating energy release rates," *Engineering Fracture Mechanics,* vol. 21, no. 2, 1985.

[52] S. Mohammadi, Extended Finite Element Method, Tehran: Blackwell, 2008.

[53] E. Giner, N. Sukumar and F. J. Fuenmayor, "An Abaqus implementation of the extended finite element method," *Engineering Fracture Mechanics,* vol. 76, no. 3, pp. 347-368, 2009.

[54] Dassaul Systèmes, ABAQUS 6.11 Documentation, 2011.

[55] M. Sabsabi, Modelado de grieta y estimación de vida en Fretting Fatiga mediante el Método de los Elementos Finitos Extendidos X-FEM, Universidad Politécnica de Valencia, 2010.

[56] American Society for Materials, ASM Handbook: Properties and Selection: Nonferrous Alloys and Special-Purpose Materials, vol. 2, 1990.

[57] Dassaul Systemes, Abaqus 6.11 Documentation, 2011.

[58] C. Song, M. X. Shen, X. F. Lin, D. W. Liu and M. H. Zhu, "An investigation on rotary bending fretting fatigue damage of railway axles," *Fatigue & Fracture of Enginnering Materials & Structures,* vol. 37, no. 1, pp. 72-84, 2014.

APPENDICES

A. Abaqus Input file template grXFEM.inp

```
*Heading
TEMPLATE FOR X-FEM WITH ABAQUS
**
** ==================================================
** (1) USER ELEMENT DEFINITION (CALLED U12, 12 DOF/NODE)
** ==================================================
*User element, nodes=4, type=U12, properties=2, iproperties=5, coordinates=2,
variables=9000
1,2,3,4,5,6,7,11,12,13,14,15
**
** ==================================================
** (2) MESH DEFINITION
** ==================================================
** -- PIECE NODES
*Node, input=.\files\m0XY.prn
** -- ONLY THE NON-ENRICHED ELEMENTS (STANDARD ELEMENTS)
*Element, type=CPE4, input=.\files\TopNoX, elset=ELEMTOPNOX
*Nset, nset=ELEMTOPNOX, elset=ELEMTOPNOX
*Solid Section, elset=ELEMTOPNOX, material=Material-1
1.
** -- INDENTER NODES
*Node, input=.\files\miXY.prn
*Element, type=CPE4, input=.\files\miTop.prn, elset=ELEMIDENT
*Nset, nset=ELEMIDENT, elset=ELEMIDENT
*Solid Section, elset=ELEMIDENT, material=Material-1
1.
** -- T2D2 NODES
**node, input=.\files\mT2D2
**Element, type=T2D2, input=.\files\TopT2D2, elset=ELEMT2D2
**Nset, nset=ELEMT2D2, elset=ELEMT2D2
**Solid Section, elset=ELEMT2D2, material=MaterOverlay
**1.
** ==================================================
** (3) USER ELEMENTS
** ==================================================
*Element, type=U12, input=.\files\TopX, elset=ELEMTOPXU12
*Nset, nset=ELEMTOPXU12, elset=ELEMTOPXU12
**
** ==================================================
** (4) NSETS & ELSETS INCLUSION
** ==================================================
** -- SETS OF NODES BELONGING TO ENRICHED ELEMENTS
*Nset, nset=NodeX2dof
*include,input=.\files\SETNodeX2dof
*Nset, nset=NodeX4dof
*include,input=.\files\SETNodeX4dof
*Nset, nset=NodeX10dof
*include,input=.\files\SETNodeX10dof
**
** -- TO INCLUDE OTHER SETS (SPECIFIC TO THE PROBLEM)
*include,input=.\files\m0sets.prn
```

```
*include,input=.\files\m0surfaces.prn
**
** ==================================================
** (5) OVERLAY ELEMENTS (if desired)
** ==================================================
*Element, type=CPE4, input=.\files\TopXoverlay, elset=ElemTopXoverlay
*Solid Section, elset=ElemTopXoverlay, material=MaterOverlay
1.
**
** ==================================================
** (6) MATERIALS DEFINITION
** ==================================================
*Material, name=Material-1
*Elastic
71E3, 0.333
*Material, name=MaterOverlay
*Elastic
1e-14, 0.300
** (negligible stiffness)
**
** -- USER DEFINED PROPERTIES FOR USER ELEMENTS. Keys:
**   1st Parameter: E (Young's modulus)
**   2nd Parameter: nu (Poisson's ratio)
**   3rd Parameter: plane stress = 1; plane strain = 2
**    4th  Parameter:  orderC(1)  =  Quadrature  order  for  quadrilaterals  non
intersected elements(in each direction)
**   5th Parameter: orderC(2) = Quadrature order for triangles (total points)
**   6th  Parameter:  orderC(3)  =  Quadrature  order  for  quadrilaterals  (in  each
direction)
**   7th Parameter: Dimension of the physical domain of the problem: 2=2D
*Uel property, elset=ELEMTOPXU12
71E3, 0.333,1,5,7,2,2
**
** ==================================================
** (7) BOUNDARY CONDITIONS
** ==================================================
**  -- T2D2 Nodes restriction
**Equation, INPUT=.\files\CalEqu
**
**  -- BC (USED IN X-FEM TO CONSTRAINT THE NON-USED EXTRA DOF)
**Boundary, OP=MOD
**NodeX2dof, 3, 15, 0.0
**NODeX4dof, 5, 15, 0.0
**NODeX10dof, 3, 4, 0.0
**
** -- OTHER BC (SPECIFIC TO THE PROBLEM)
**
** -- CONTACT DEFINITION
*Surface Interaction, name=IntProp-2
1.,
*Friction, lagrange
0.8
*Contact Pair, interaction=IntProp-2, SMALL SLIDING
SLAVEC,MASTERC
** ==================================================
```

```
** (8) LOAD STEPS
** ==================================================
**
** STEP: Step-1
*Step, unsymm=YES
Step-1-Pload: Normal load application
** -- WE DON'T USE *Static. WE USE THE FOLLOWING TO USE DOFS 1-7 & 11-15
*coupled temperature-displacement, steady state
0.25, 1., 1e-05, 0.25
*Contact Controls, friction onset=immediate
**
** -- Specific loads in the analysis
**
** ==================================================
** (9) OUTPUT FILES
** ==================================================
** -- OUTPUT FIELD TO .odb
*Output, field, op=NEW, frequency=1
*Node Output
U
*Element Output
S, E
*Contact Output
CSTRESS, CDISP
** -- OUTPUT PRINT TO .dat
** -- 'U' TO LIST DOFS 1-7 & 'NT' TO LIST TEMP. ASSOCIATED DOFS 11-...
*Node print, nset=ELEMTOPXU12,frequency=1
U
*Node print, nset=ELEMTOPXU12,frequency=1
NT
** -- OUTPUT WRITE TO  .fil
*Node file, nset=ELEMTOPNOX
COORD,U
*EL FILE, elset=ELEMTOPNOX, POSITION=AVERAGED AT NODES
S,
*El file, elset=ELEMTOPNOX, POSITION=INTEGRATION POINT
S,E,ENER,IVOL
** -- TO WRITE USER DEFINED OUTPUT VARIABLES FOR POST-PROCESSING
** -- (INFORMATION AT GAUSS POINTS OF ENRICHED ELEMENTS)
*El file, elset=ELEMTOPXU12
SDV
**
*Output, history
*Contact file, frequency=1, slave= SURF-SLAVE
CSTRESS, CDISP
**
*Output, history
*Contact Output
CSTRESS, CDISP
**  RESULTS FILE en .dat
**
*Contact print, frequency=1, slave= SURF-SLAVE
CSTRESS, CDISP
**
*End Step
```

**

B. User element routine template UEL_XFEM.for

```
      SUBROUTINE UEL(RHS,AMATRX,SVARS,ENERGY,NDOFEL,NRHS,NSVARS,
     * PROPS,NPROPS,COORDS,MCRD,NNODE,U,DU,V,A,JTYPE,TIME,DTIME,
     * KSTEP,KINC,JELEM,PARAMS,NDLOAD,JDLTYP,ADLMAG,PREDEF,NPREDF,
     * LFLAGS,MLVARX,DDLMAG,MDLOAD,PNEWDT,JPROPS,NJPROP,PERIOD)
C
      INCLUDE 'ABA_PARAM.INC'
C
C     User subroutine for computation of element stiffness matrix
C     and the element force vector
C
C     ABAQUS defined variables
C
      DIMENSION RHS(MLVARX,*), AMATRX(NDOFEL,NDOFEL), PROPS(*),
     * SVARS(NSVARS), ENERGY(8), COORDS(MCRD,NNODE), U(NDOFEL),
     * DU(MLVARX,*), V(NDOFEL), A(NDOFEL), TIME(2), PARAMS(*),
     * JDLTYP(MDLOAD,*), ADLMAG(MDLOAD,*), DDLMAG(MDLOAD,*),
     * PREDEF(2,NPREDF,NNODE), LFLAGS(*), JPROPS(*)
C
C     main subroutine variables
C          JELEM  Número current element
C          F      Element force vector
C           AMATRX Element stiffness matrix
C          E:     Young´s modulus
C          Nu:    Poisson´s ratio
C          TDP:   1 - Plane stress
C                 2 - Plane strain
C          orderC quadrature order for elements:
c                   orderC(1) quadrature order for cuadrilaterals(non
intersected elements)
C              orderC(2) quadrature order for triangles orden de cuadratura en
triángulos (nº ptos totales
c              orderC(3) quadrature order for cuadrilaterals
c          dimens Dimensions of the physical domain
C          NPG    Number of crack path points
C          NelmX  Number of enriched elements
C          NnodX  Number of enriched nodes
C          TipoXe Vector that stores the key in TypeX for the nodes in the
current element
c          ix     Vector that stores the current element topology
C          XYG    Matrix that stores the Crack path points
C          lint   Number of integration points in teh current element
C          flag   Subdivision indicator
C          mpg    Maximum number of Gauss point in a enriched element
C          sg     Matrix that stores the Gauss point coordinates and weights
c          Xe     Abscissa nodal coordinates of the current element
c           Ye     Ordinate nodal coordinates of the current element
c                     (Se utilizan duplicados para facilitar los contadores
```

```
C       User defined variables
C
        REAL*8 E, Nu
        REAL*8 F(NDOFEL)
        INTEGER i,j,k,TDP,orderC(3),lint,flag,dimens
        integer NPG,NelmX,NnodX,TipoXe(NNODE),ix(NNODE)
        integer,parameter :: mpg=50
        real*8 sg(3,mpg),xypg(2,mpg),Xe(8),Ye(8)
         INTEGER,ALLOCATABLE:: TipoX(:,:)
         REAL*8, ALLOCATABLE:: XYG(:,:),Dist(:,:),ElemGG(:,:)
        REAL*8, ALLOCATABLE:: BenG(:,:),DBenG(:,:),JenG(:)
C       &&&&&&&&&&&&&&&&&&&&&&&&&&&&&&&&&&&&&&&&&&&&&&&&&&&&&&&&&&&&&&&&
C       &&&&&&&&&&&&&&&&&&&&&&&&&&&&&&&&&&&&&&&&&&&&&&&&&&&&&&&&&&&&&&&&
C       &&&&&&&&&&&&&&&&&&&&&&&&&&&&&&&&&&&&&&&&&&&&&&&&&&&&&&&&&&&&&&&&

C       Real and integer properties defined in Abaqus
        E = PROPS(1)
        Nu = PROPS(2)
        TDP = JPROPS(1)
        orderC(1) = JPROPS(2)
        orderC(2) = JPROPS(3)
        orderC(3) = JPROPS(4)
        dimens = JPROPS(5)
C       Read current directory
        CALL GETOUTDIR(OUTDIR,LENOUTDIR)

        OPEN(68,FILE=OUTDIR(1:LENOUTDIR)//'\files\GGInfoX')
         READ(68,*) NPG,NelmX,NnodX
         CLOSE(68)

c       Read previously preprocessed information

        allocate (TipoX(NnodX,2))
        allocate (XYG(NPG,2), Dist(NnodX,3), ElemGG(NelmX,8))

         OPEN(68,FILE=OUTDIR(1:LENOUTDIR)//'\files\GGXYC')
        do i=1,NPG
          READ(68,*) (XYG(i,j),j=1,2)
        end do
         CLOSE(68)

         OPEN(68,FILE=OUTDIR(1:LENOUTDIR)//'\files\GGnodeX')
        do i=1,NNodX
          READ(68,*) (TipoX(i,j),j=1,2),(Dist(i,j),j=2,3)
          Dist(i,1)=TipoX(i,1)
         end do
         CLOSE(68)

        OPEN(68,FILE=OUTDIR(1:LENOUTDIR)//'\files\GGelemX')
        do i=1,NelmX
          READ(68,*) (ElemGG(i,j),j=1,8)
         end do
         CLOSE(68)

       call inicializaM(RHS,NDOFEL,NRHS)
```

```
      call inicializaM(AMATRX,NDOFEL,NDOFEL)
      call inicializaV(ENERGY,8)
      call inicializaV(SVARS,NSVARS)

c     element type verifiaction

       IF (JTYPE.EQ.12) THEN
C       *********************************
C       *  4 NODE ENRICHED ELEMENT WITH *
C       *  UP TO 12 DOF/NODE FOR X-FEM  *
C       *********************************
         IF (LFLAGS(3).EQ.1) THEN
C        User subroutine must define the residual vector F and the stiffness
matrix

c        Subroutine that defines the location of integration points
           call int2d_X(JELEM,NelmX,ElemGG,MCRD,NNODE,COORDS,orderC,
     *                  NPG,XYG,lint,sg,Xe,Ye,flag,mpg,xypg)

            ALLOCATE(BenG(3*lint,NDOFEL),DBenG(3*lint,NDOFEL),JenG(lint))
         call inicializaM(BenG,3*lint,NDOFEL)
            call inicializaM(DBenG,3*lint,NDOFEL)
            call inicializaV(JenG,lint)

c       Soubroutine that search the node numbers of the current element and his
enrichment
c       flag (TipoX) and store it in TipoXe
         call TipoXelemento(OUTDIR,LENOUTDIR,JELEM,NNODE,NelmX,
     *                   ix,TipoXe)

c           Subroutine that define the element stiffness matrix
          CALL K_U12(E,Nu,AMATRX,NDOFEL,NNODE,dimens,MCRD,
     *              COORDS,TDP,NnodX,ix,TipoXe,Dist,NPG,XYG,lint,sg,
     *               Xe,Ye,flag,BenG,DBenG,JenG)



C       Subroutine that found important information in the Gauss points (strain,
stress, etc.)
           CALL  SVARS_U12(JTYPE,JELEM,SVARS,NSVARS,U,NDOFEL,BenG,
     *                    DBenG,JenG,lint,mpg,xypg)
          END IF
        END IF
C
```

C. Element stiffness matrix subroutine template K_U12

```
      SUBROUTINE K_U12(E,Nu,AMATRX,Dof,nel,ndm,MCRD,COORDS,
     *          TDP,NnodX,ix,TipoXe,Dist,NPG,XYG,lint,sg,Xe,Ye,
     *          flag,BenG,DBenG,JenG)
```

```
      IMPLICIT NONE

c         nel           Number of nodes per element
c         ix(nel)       Element topology
c         TipoXe(nel)   Nodes enrichment flag (0,1 o 2)
c
c     Variable definition
      integer dfich,dfich2
      common /debugfich/ dfich,dfich2
       INTEGER Dof, nel, ndm, MCRD, TDP, NnodX,NPG,lint,flag,pos
       INTEGER TipoXe(nel),ix(nel)
      REAL*8 E, Nu,Dist(NnodX,3),XYG(NPG,2),sg(3,*)
       REAL*8 K(Dof,Dof)
      REAL*8 Xe(2*nel),Ye(2*nel),COORDS(MCRD,nel),xl(ndm,nel)
       REAL*8 xsj(lint),shp(3,16,lint)
       REAL*8 dFI(nel,2,4),dFInodo(nel,2,4),H,Hnodo(nel)
      REAL*8 Be(3,Dof), DB(3,Dof), BT(Dof,3), D(3,3)
      REAL*8 BenG(3*lint,Dof),DBenG(3*lint,Dof),JenG(lint)
       logical HayNodoTipo1,HayNodoTipo2
       integer l,i,j,kk

c     Pass information from 3D to 2D
      do i=1,ndm
        do j=1,nel
          xl(i,j)=COORDS(i,j)
       end do
      end do

c     Subroutine that define the constitutive stress-strain elastic matrix
       CALL CALC_D(TDP,D,E,Nu)

c     Specify the type of nodal enrichment

       do i=1,nel
           if (TipoXe(i).eq.1) then
             HayNodoTipo1=.true.
           elseif (TipoXe(i).eq.2) then
             HayNodoTipo2=.true.
           endif
       end do


c       Numerical integration loop over the gauss points (gint)

        do l = 1,lint

c            Soubroutine the define the shape functions and derivatives
        call shp2d(sg(1,l),xl,shp,xsj(l),ndm,nel,ix,.false.)

             if (flag.eq.1) then       !Element is subdivided for integration
            xsj(l) = sg(3,l)      !The integration weights include the Jacobian
             else                      !Element is not subdivided
               xsj(l) = xsj(l)*sg(3,l) !Standard integration
             endif
```

```
c       Compute stresses and strains
c            Heaviside function calculation at Gauss and nodal points
             if (HayNodoTipo1) then
               call Heaviside(NnodX,Dist,nel,ix,shp,H,Hnodo)
             endif

c       Crack tip derivates calculation at Gauss and nodal points
        if (HayNodoTipo2) then
               call fCrackTip(NPG,XYG,shp,Xe,Ye,dFI,dFInodo)
             endif

c       Stiffness matrix computation

               Pos=1
c              Loop over the nodes
               do i= 1,nel

c       Contribution to B of derivatives of standard shape functions
                    Be(1,Pos)  = shp(1,i,1)
                    Be(2,Pos+1)= shp(2,i,1)
                    Be(3,Pos)  = shp(2,i,1)
                    Be(3,Pos+1)= shp(1,i,1)



c       Contribution to B of derivatives of shape functions times Heaviside
function
                  if (TipoXe(i).eq.1) then
                    Be(1,2+Pos)  = (H-Hnodo(i))*shp(1,i,1)
                    Be(2,3+Pos)  = (H-Hnodo(i))*shp(2,i,1)
                    Be(3,2+Pos)  = (H-Hnodo(i))*shp(2,i,1)
                    Be(3,3+Pos)  = (H-Hnodo(i))*shp(1,i,1)


c       Contribution to B of derivatives of shape functions times crack tip
functions
                  elseif(TipoXe(i).eq.2) then
                    do kk= 1,4
                      Be(1,2*kk+2+Pos)= dFI(i,1,kk)-dFInodo(i,1,kk)
                     Be(2,2*kk+3+Pos)= dFI(i,2,kk)-dFInodo(i,2,kk)
                      Be(3,2*kk+2+Pos)= dFI(i,2,kk)-dFInodo(i,2,kk)
                      Be(3,2*kk+3+Pos)= dFI(i,1,kk)-dFInodo(i,1,kk)
                    end do
                  end if


                  Pos=Pos+12 ! Each node has 12 DOF

               end do !  End loop over the element nodes

c              D*B Matrix
               DB=matmul(D,Be)
c              B Tranpose matrix
               BT=transpose(Be)
```

```
c              Matriz de rigidez integrando Bt*D*B
               AMATRX=AMATRX+ matmul(BT,DB)*xsj(l)


c         Store information at each integration point for further post-
processing
            do  i=1,3
              do j=1,Dof
               BenG(3*(l-1)+i,j)=Be(i,j)
               DBenG(3*(l-1)+i,j)=DB(i,j)
              end do
              end do
            JenG(l)=xsj(l)



        end do ! End loop over the integrations points


      RETURN
      END
```